May 2013

Low Turbulence Wind Tunnel Design and Wind Turbine Wake Characterization

Andrew Welsh
University of Wisconsin-Milwaukee

LOW TURBULENCE WIND TUNNEL DESIGN AND WIND TURBINE WAKE CHARACTERIZATION

by

Andrew Welsh

A Thesis Submitted in

Partial Fulfillment of the

Requirements for the Degree of

Master of Science

in Engineering

at

The University of Wisconsin-Milwaukee

May 2013

ABSTRACT

LOW TURBULENCE WIND TUNNEL DESIGN AND WIND TURBINE WAKE CHARACTERIZATION

by

Andrew Welsh

The University of Wisconsin-Milwaukee, 2013

Under the Supervision of Professor Amano

As the prevalence of wind turbines in the energy market increases, so too does the demand for high-wind real-estate. As a result, wind turbines are placed closer together, which leads to structural challenges due to the cyclical fatigue loading from the wake of upwind turbines. Characterizing the wake behind wind turbines with respect to those downwind is especially important given the 20-year wind turbine lifetime that commercial wind turbine consumers expect. This project aimed to characterize the near wake behind a model wind turbine.

In order to accomplish this, a 12.8 meter-long and 1.22 meter-square test section low-turbulence wind tunnel and a 30 cm-diameter three-blade NACA 4412 wind turbine were designed and constructed. Velocity was measured using a 2-axis X-type miniature hotwire anemometer attached to a three axis traverse, which was controlled with LabVIEW 2012. Data acquisition was programed in LabVIEW 2012, and data reduction was performed in MATLAB.

The near wake characterization showed steep velocity gradients, which are indicative of high turbulence, directly behind the wind turbine hub and at the blade tips. At 3 blade diameters downstream from the wind turbine, the beginning of the transition to the far wake could clearly

be seen. The previously steep velocity gradients at the blade tips became more diffuse and the large velocity gradients were centered behind the hub. This followed the bell-shaped turbulence intensity curve theory predicts. In the far wake-region turbulence will collapse toward the center of the wind turbine wake and turbulence at the blade tips will expand out and return to ambient.

The data collected matched both theoretical computational fluid dynamics as well as previous experimental results. This work validates and opens the door to the use of the wind tunnel for future work to refine the wake characterization and the prediction of cyclical loading on downwind wind turbines.

TABLE OF CONTENTS

LIST OF FIGURES

LIST OF TABLES

NOMENCLATURE

$$Contraction\ Ratio = \frac{Inlet\ Cross\ Sectional\ Area}{Outlet\ Cross\ Sectional\ Area} \quad (1)$$

$$Diffuser\ Area\ Ratio = \frac{Outlet\ Area}{Inlet\ Area} \quad (2)$$

$$f = \frac{turbulence\ with\ manipulators}{turbulence\ without\ manipulators} = Turbulence\ Reduction\ Factor \quad (3)$$

$$\Delta H_l = P_1 - P_2 \quad (4)$$

$$I = \frac{U'}{U}\ \ Or\ \ \frac{V_{Max} - V_{Min}}{V_{Avg}} = Turbulence\ Intensity \quad (5)$$

$$I_{add} = Additional\ Tubulence\ Intensity\ Caused\ by\ Wind\ Turbine \quad (6)$$

$$I_{ave} = Average\ Turbulence\ Intensity \quad (7)$$

$$I_0 = Ambient\ Turbulence\ Intensity \quad (8)$$

$$K_l = \frac{\Delta H_l}{(\frac{1}{2})\rho_1 V_1^2}\ (Assuming\ Incompressable\ Flow) \quad (9)$$

$$K_l\ =\ Loss\ Coefficient \quad (10)$$

$$P_1 = Upstream\ Static\ Pressure \quad (11)$$

$$P_1 + \left(\frac{1}{2}\right)\rho_1 V_1^2 = P_2 + \left(\frac{1}{2}\right)\rho_2 V_2^2\ (Bernouli's\ Equation) \quad (12)$$

$$P_2 = Downstream\ Static\ Pressure \quad (13)$$

$$\rho_1 = Upstream\ density \quad (14)$$

$$\rho_2 = Downstream\ density \quad (15)$$

$$U = Mean\ of\ velocity\ of\ time\ varrying\ wind\ field \quad (16)$$

$$U' = Standard\ deviation\ of\ velocity\ of\ time\ varrying\ wind\ field \quad (17)$$

$$U_t = Average\ Test\ Section\ Flow\ Velocity \quad (18)$$

$$V_1\ = Upstream\ Velocity \quad (19)$$

$$V_2\ = Downstream\ Velocity \quad (20)$$

$V_{Avg} =$ Maximum flow velocity (21)

$V_{Max} =$ Maximum flow velocity (22)

$V_{Min} =$ Maximum flow velocity (23)

ACKOWLEDMENTS

Thank you Dr. Amano for your help and support throughout this process!

Introduction:

As the prevalence of wind turbines in the energy market increases, demand for high wind real estate goes up. As a result, wind turbines are being placed closer and closer together leading to unique structural challenges due to cyclical fatigue loading from the wake of upwind wind turbines. Characterizing the wake behind wind turbines with respect to downwind wind turbines is especially important given the 20 year wind turbine lifetime that commercial wind turbine consumers expect.

Extensive research is being conducted on the wake behind wind turbine blades due to increased pressure on green technologies. This, coupled with a dramatic increase in computer power, has enabled advanced experimental and theoretical research on the wake behind wind turbines.

Shear from steep velocity gradients the predominant cause of turbulence in wind turbine wake [1]. Air passing near wind turbine blades has a large reduction in axial velocity and also has a high increase in radial velocity. In contrast, air flowing through the wind turbine, in time periods where no blades pass, retains much of its initial velocity. Additionally, air passing to the outside of the wind turbine flows at ambient air velocity. These flow characteristics cause steep velocity gradients that lead to turbulence. Other sources of turbulence in wind turbine wake include preexisting ambient turbulence and turbulence due to the hub.

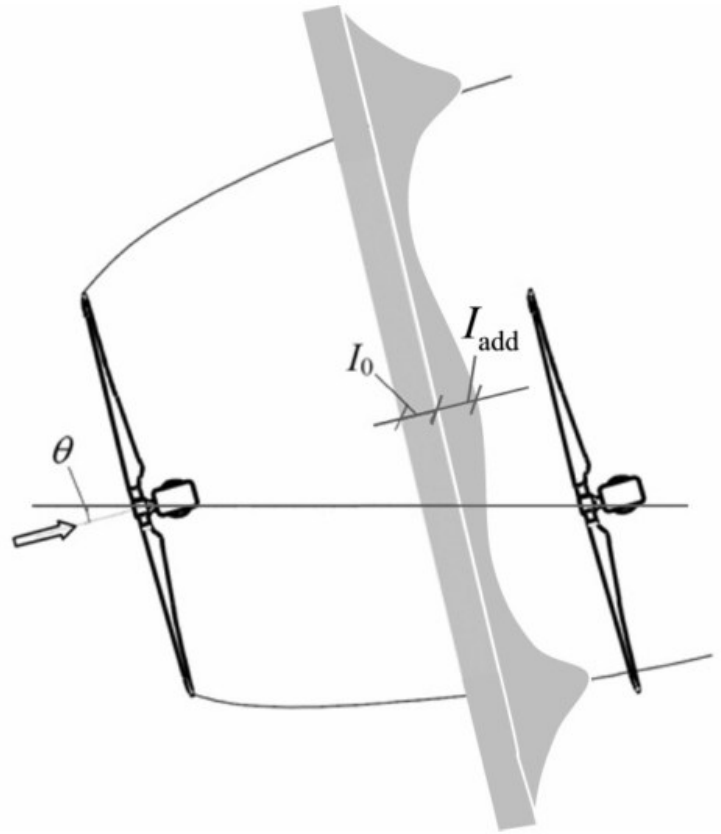

Figure 1. Distribution of turbulence intensity in the near-wake [1]

As can be seen in **Error! Reference source not found.**, initially turbulence generated by the blade tip vortices and the hub are separate from each other.

This is characteristic of the near wake region which is generally accepted to be as long as between 3 and 5 rotor diameters downwind of the wind turbine. The near wake is the region this paper will be predominately focused on. Turbulence on the outside edges of the blade, nearest to ambient, dissipates into heat while the majority of the turbulence collapses toward the center of the wake creating the bell shaped curve shown in Figure 2.

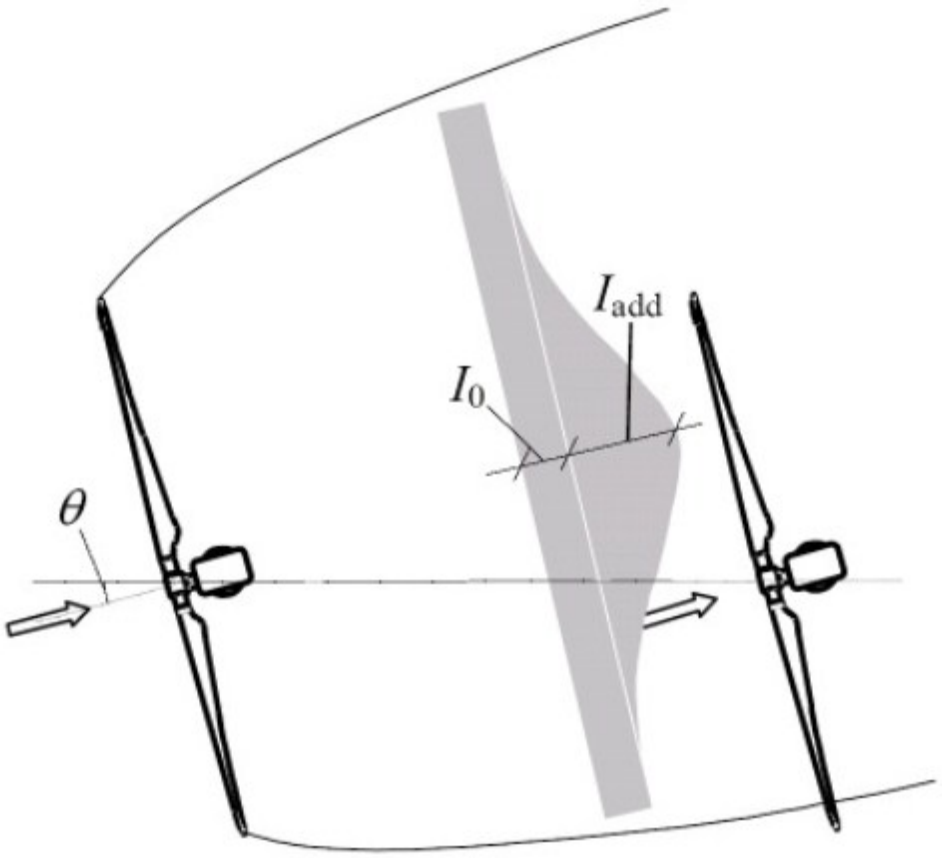

Figure 2. Distribution of turbulence intensity in the far-wake [2]

A bell shaped turbulence distribution is characteristic of the completion of the transformation between the near and far wake regions. In the far wake region turbulence is converted into heat as the flow returns to ambient.

An effective characterization of the severity of the turbulence in the wake behind wind turbines is the turbulence intensity. Turbulence intensity is the standard deviation of the fluid velocity divided by the average velocity of the fluid where "turbulence can be described as eddies which dissipate through transferring energy from larger to smaller eddies and then to heat." [2].

Turbulence intensity is assumed to be additive and can be superimposed. The ambient turbulence intensity, I_0, can therefore be removed from the total turbulence intensity leaving only the turbulence intensity caused by the wind turbine, I_{add}. Relative turbulence intensity, the ratio of the turbulence intensity in the wake to the turbulence intensity upstream of the wind turbine is given below in Figure 3 for an ENERCON E66 wind turbine at 2.06 blade diameters downwind.

The data graphed was collected by the Dutch Institute for Structural Engineering and was presented in "Dynamic Loads in Wind Farms I" [3]. Both the measured data and the simulated, data using a RANS approach, show the blade tip vortices still separated from the rest of the turbulence in the near wake region.

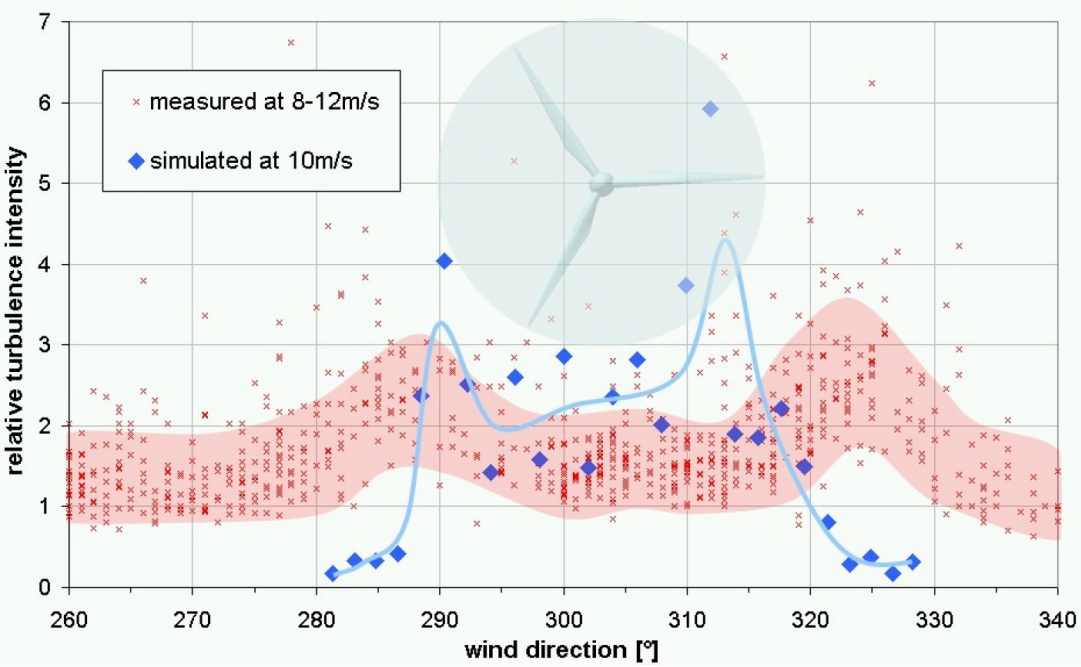

Figure 3. Relative turbulence intensity at 2.06 blade diameters [3]

Researchers at the fluid mechanics laboratory at ENSAM-Paris used particle image velocitometry and hot wire anemometry to characterize the near wake behind a

modified Marlec Rutland 503 wind turbine in a wind tunnel [2]. The rotor diameter of the wind turbine was 500mm, the rotational velocity was 1050 rpm, and the wind velocity was 9.3 m/s. Phase locked, ensemble averaging techniques were used to capture time specific flow phenomena. Blade tip vortices can clearly be seen in Figure 4 up to one rotor diameter downwind and the transition to a bell shaped flow structure can be seen at 1.5 diameters. The transition from near to far wake is accelerated in a wind tunnel due to wall effects. Again, in an infinite field, research shows this transition occurs at roughly 5 rotor diameters.

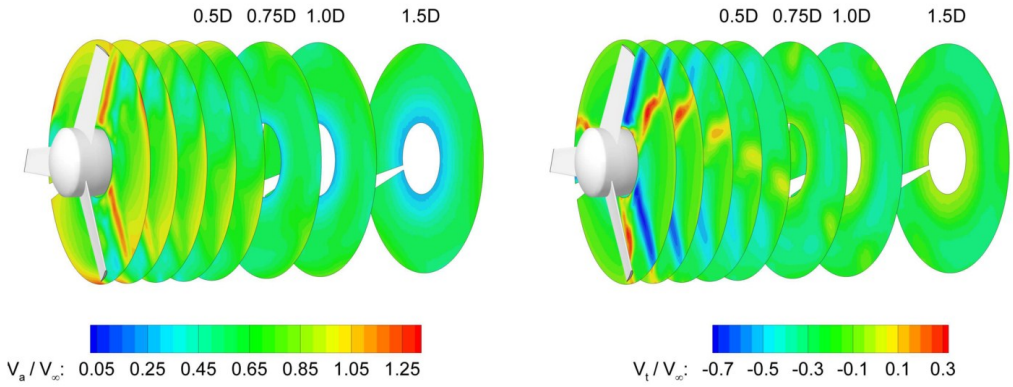

Figure 4. Contour of near wake axial velocity, left, and tangential velocity, right [4]

Additionally, the near wake region of a scale wind turbine in a wind tunnel will differ from that of a full scale commercial wind turbine due to the "difference in turbulence mixing between in the wind tunnel and in the atmospheric surface boundary layer" [5].

These results match very closely with those found in Figure 5 where Large Eddy Simulations (LES) and experimental results were compared for a 30 meter diameter wind turbine in the Sevierum wind farm.

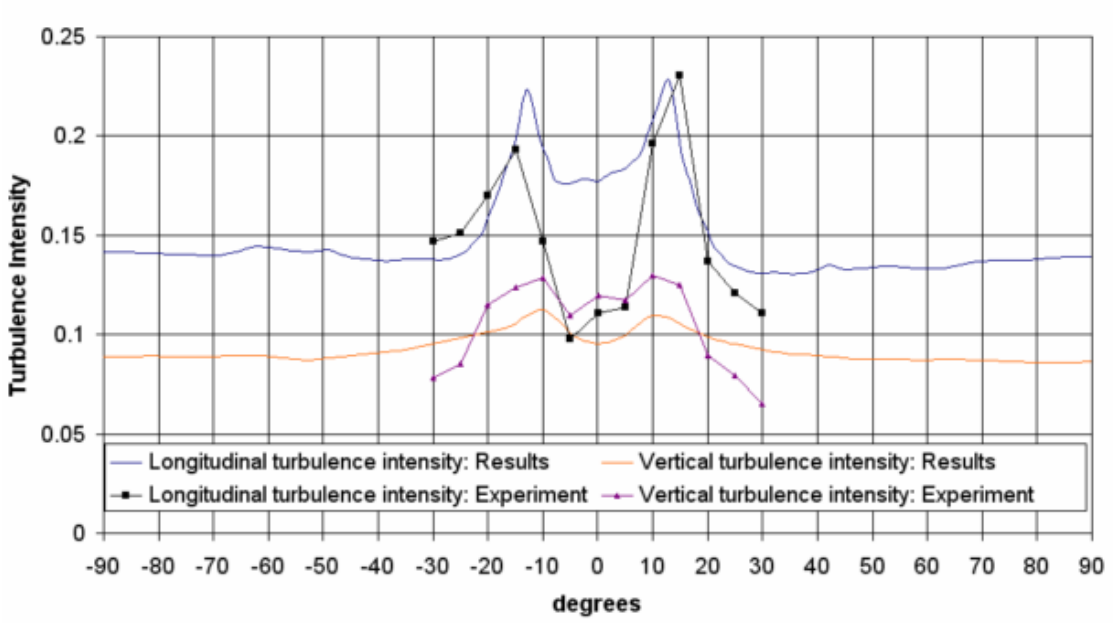

Figure 5. Experimental and CFD (LES) turbulence intensity at 2.5 turbine diameters [6]

The same LES results were extended to the far wake in Figure 6. Clear differentiation of the vortices can be seen from the rest of the wake in the near wake region. The wake degrades to a bell curve by five rotor diameters.

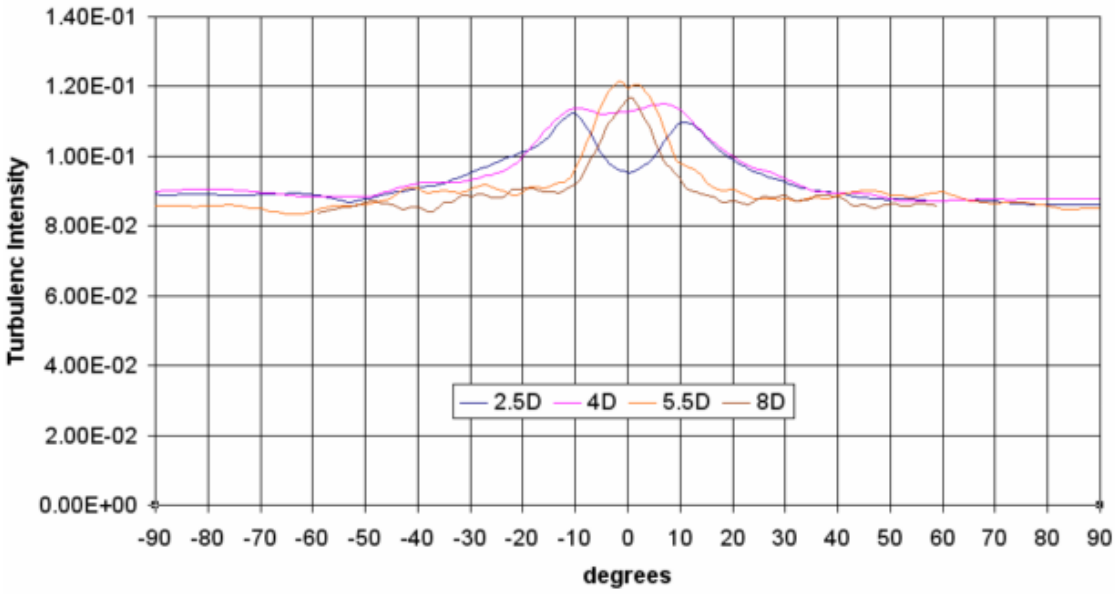

Figure 6. CFD (LES) turbulence intensity at 2.5, 4, 5.5 and 8 turbine diameters [6]

Experimental Design:

It was chosen to focus primarily on obtaining an experimental characterization of the wake distribution in the near wake region behind a model wind turbine for this paper. CFD results were extensively investigated but were not pursued.

To facilitate experimental research on the wake behind a model wind turbine, a research grade low-turbulence wind tunnel was designed and built. In addition, a 60.96 cm diameter, three NACA 4412 blade, model wind turbine was designed and built. Turbulence intensity was measured using a 2-D X-Type DANTEC Micro Hotwire Anemometer in conjunction with a custom built Velmex three axis traverse. National Instruments hardware and software were used for data acquisition and control. The design of each of these components will be discussed in the following sections.

Wind Tunnel Design and Components:

There are many different types and sizes of wind tunnels currently in use, each with unique advantages and disadvantages. The wind tunnel designed for this experiment is a low turbulence, 12.8 meter long, suck-through type wind tunnel with a 1.22 meters square test section that is 2.44 meters long. A low turbulence wind tunnel eliminates twist in the incoming air and significantly reduces the amount and scale of turbulence entering the test section. The major components of a low turbulence wind tunnel are as follows (in order from the wind tunnel inlet to outlet).

1) Honeycomb - Eliminates twist in flow
2) Screens - Reduces amount and scale of turbulence
3) Settling Distance - Allows flow to stabilize before entering contraction section

4) Contraction Section - Reduces the scale of turbulence and increases flow velocity

5) Test Section - Low turbulence testing area

6) Diffuser - Transitions the test section cross section to the fan cross section.

7) Safety Fence - Reduces chance of test section debris impacting the fan

8) Fan/Diffuser Coupling - Prevents fan vibration from spreading to the test section

9) Fan - Pulls air through the wind tunnel

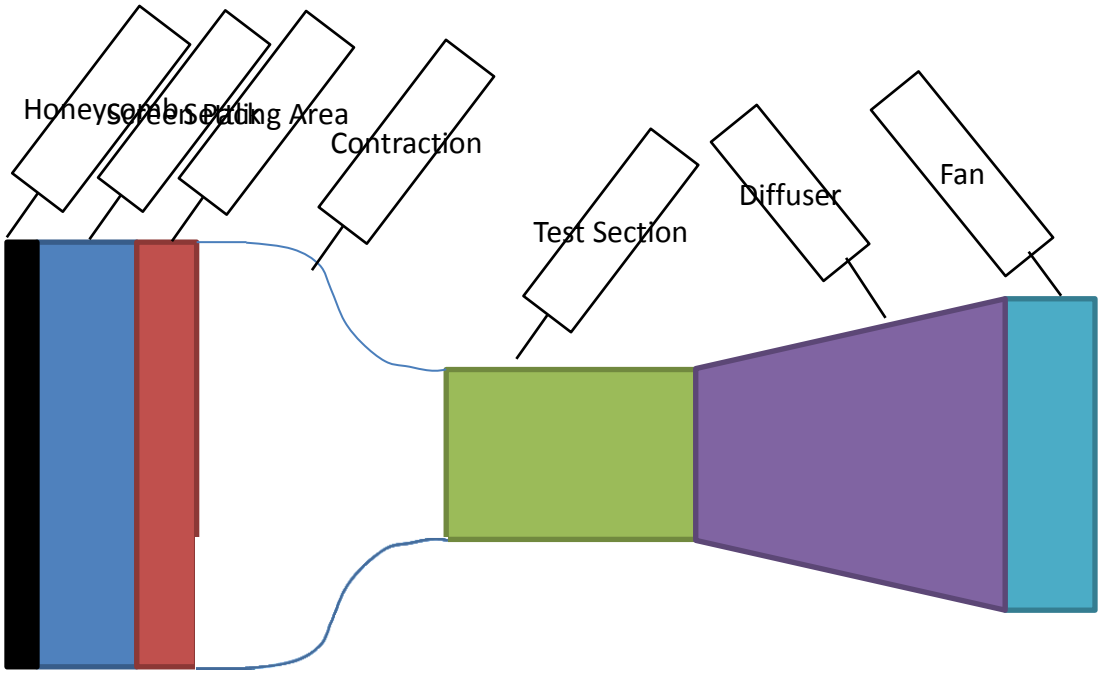

Figure 7. Basic wind tunnel schematic

General Wind Tunnel Type Design:

There are two main categories of wind tunnels. The first is open circuit, Eiffel-Type, wind tunnels where flow enters from and exits to atmospheric. The name "Eiffel-Type" was obtained due to this wind tunnel category's resemblance to the Eiffel Tower as can

be seen in Figure 6. The second type of wind tunnel is a closed circuit recirculating wind tunnel where the flow is enclosed at all times.

Eifel-Type wind tunnels are advantageous in that they use significantly less space than a recirculating wind tunnel. In addition, wind tunnel generated heat is dissipated to the room leading to much steadier flow temperatures. This is very important in hotwire measurements.

The advantages of a recirculating wind tunnel are higher flow velocities due to lower momentum loss and lower turbulence due to the flow being reconditioned each time it passes the flow conditioning section of the wind tunnel (honeycomb, screens, etc.). However, recirculating wind tunnels generate significant heat which requires expensive heat exchangers to keep flow temperature constant. Recirculating wind tunnels also require flow conditioners at each corner to ensure low turbulence development and pressure losses. In addition, they also require more powerful fans due to the increased mass flow and take up significantly more space than Eiffel-Type wind tunnels.

Both Eiffel-Type and recirculating wind tunnels are divided into two categories, “suck-through” and “blow-down”. The designations are based on fan orientation in relation to the flow conditioning and test sections. If the fan is after the test section and is pulling air through the flow conditioners and test section, then it is a suck-through type wind tunnel. If the fan is before the flow conditioners and pushes air through the flow conditioners and test section, then it is a blow-down type wind tunnel. In a recirculating

wind tunnel these definitions ban be ambiguous, but fan proximity to test section and flow conditioners makes the designation clear.

Blow-down type wind tunnels tend to cause twist in the flow that is significant enough to exist past the flow conditioning sections and into the test section. Suck-through type wind tunnels pull air with significantly less twist through the flow conditioners and have negligible twist in the test section.

An open circuit suck through wind tunnel was chosen due to steadier room temperatures for hotwire measurements, space constraints, and funding constraints on the additional materials required for a closed circuit wind tunnel. Suck-through was chosen due to the lower chance of flow twist in the test section.

Wind Tunnel Component Theory and Design Decisions:

The first major section of the wind tunnel is the flow conditioning section consisting of a honeycomb, screens, and a settling chamber. Each of these sections play a role in reducing the intensity and scale of turbulence in the flow. The screens and honeycomb must be in the lower velocity portion of the wind tunnel as low velocity air flowing through screens induces a lower pressure drop to the wind tunnel system because air can flow freely through a screen at low velocity. However, high velocity air flowing through a screen would induce a high pressure loss to the system and would significantly lower the maximum wind speed of the wind tunnel. Additionally, screens have been found to flex distances greater than 30 cm in the center in poorly designed

wind tunnels. Screen tearing and replacement is a common issue if not designed correctly.

Honeycomb:

The honeycomb is generally the first component that the flow encounters in an open circuit, suck through wind tunnel. Its purpose is to reduce large scale turbulence in the flow and remove twist from the incoming air. Honeycombs are also referred to as flow straighteners as in the process of removing twist from the flow, the honeycomb redirects all flow down the axis of the wind tunnel. Three typical styles of honeycomb are given below in Figure 8.

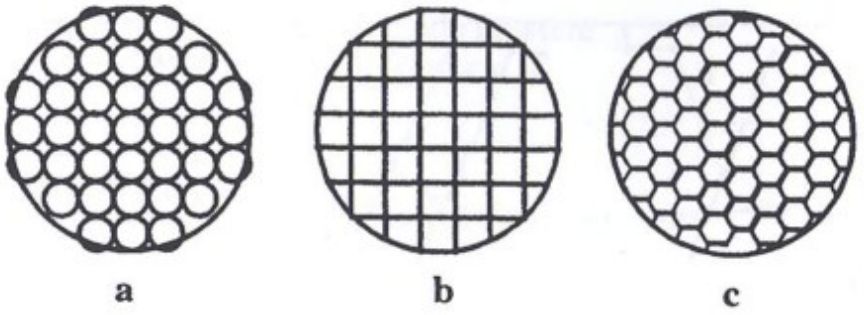

Figure 8. Honeycomb types [7]

Table 1. Pressure loss coefficients [7]

Honeycomb Type:	**Loss Coefficient (K_l):**
a	0.30
b	0.22
c	0.2

Table 1 gives the loss coefficient, K_l , for each of the honeycomb types given in Figure 8. The loss coefficient is the ratio of the pressure loss in the wind tunnel section to the dynamic pressure at the entrance of the wind tunnel section. As can be seen, hexagonal honeycombs incur the lowest pressure losses and are the most efficient for wind tunnel turbulence reduction.

The size of the honeycomb hexagons vary from wind tunnel to wind tunnel. Bradshaw and Mehta [8] found that the minimum number of cells (hexagons) is proportional to the inlet diameter of the wind tunnel. The minimum number of recommended cells is roughly 150 cells per inlet diameter, or 25,000 total cells. This is a good rule of thumb for small wind tunnels; however, large wind tunnels require significantly higher cell counts per inlet diameter. Bradshaw and Mehta also found in that the length of each cell should be 6-8 times the cell diameter.

Optimum honeycomb axial length was studied by Loehrke and Nagib [9]. When flow enters the honeycomb, the honeycomb itself induces turbulence in the flow. The length of the honeycomb acts as a settling distance where small scale turbulence dissipates into heat. However, if a honeycomb section is too long, the boundary layer in each honeycomb cell grows and the pressure loss of the wind tunnel system becomes substantial thus reducing the maximum test section velocity. Bradshaw and Mehta recommend that honeycombs with shorter axial lengths are better. They induce a smaller pressure loss to the system and generate less turbulence.

Loehrke and Nagib found that the flow out of the honeycomb was much less turbulent if the incoming flow was more turbulent with small length scale turbulence. A screen was introduced directly in front of the honeycomb which, from a single honeycomb cell's frame of reference, induced small scale turbulence that delayed boundary layer onset and increased the rate at which the flow normalized in the cell. This allowed smaller honeycomb widths to achieve greater turbulence reductions. In addition, Loehrke and Nagib found that a screen placed on the outlet of the honeycomb induces small length scale turbulence which reduces large scale turbulence, caused by the honeycomb, faster.

It was chosen to use a honeycomb with a 0.15 cm maximum hexagonal width and a 7.62 cm axial length. For the 3.05 m square wind tunnel inlet described later in the paper, this yields roughly 200 cells per flow conditioning section diameter which is greater than the 150 cell per diameter minimum recommended by Bradshaw and Mehta. The 7.62 cm axial length yields a length to cell diameter ratio between 5 and 6 which is beneficial for low pressure losses and low turbulence generation. In addition, one 24 mesh screen was placed at the inlet and outlet of the honeycomb as is recommended by Loehrke and Nagib.

Screens:

To further reduce the amount of turbulence in the flow, Scheiman and Brooks [10] recommend a series of turbulence reducing screens. Each screen increases the turbulence reduction through a combination of decreasing the scale of the turbulence

and inducing small scale turbulence into the flow. Small scale turbulence interferes with large scale turbulence in the flow and aids in dissipating turbulence to heat faster.

The screens are recommended to go from a low mesh size for the first screens to a high mesh size for the final screens. That is the screens should have a less dense mesh at the inlet of the series of screens and a more dense mesh at the outlet. It was found that the turbulence reduction factor, f as shown below in equation 1, is reduced with higher screen mesh sizes as shown below in Figure 9. A low f indicates a greater turbulence reduction.

$$f = \frac{turbulence\ with\ manipulators}{turbulence\ without\ manipulators} = Turbulence\ Reduction\ Factor \quad (1)$$

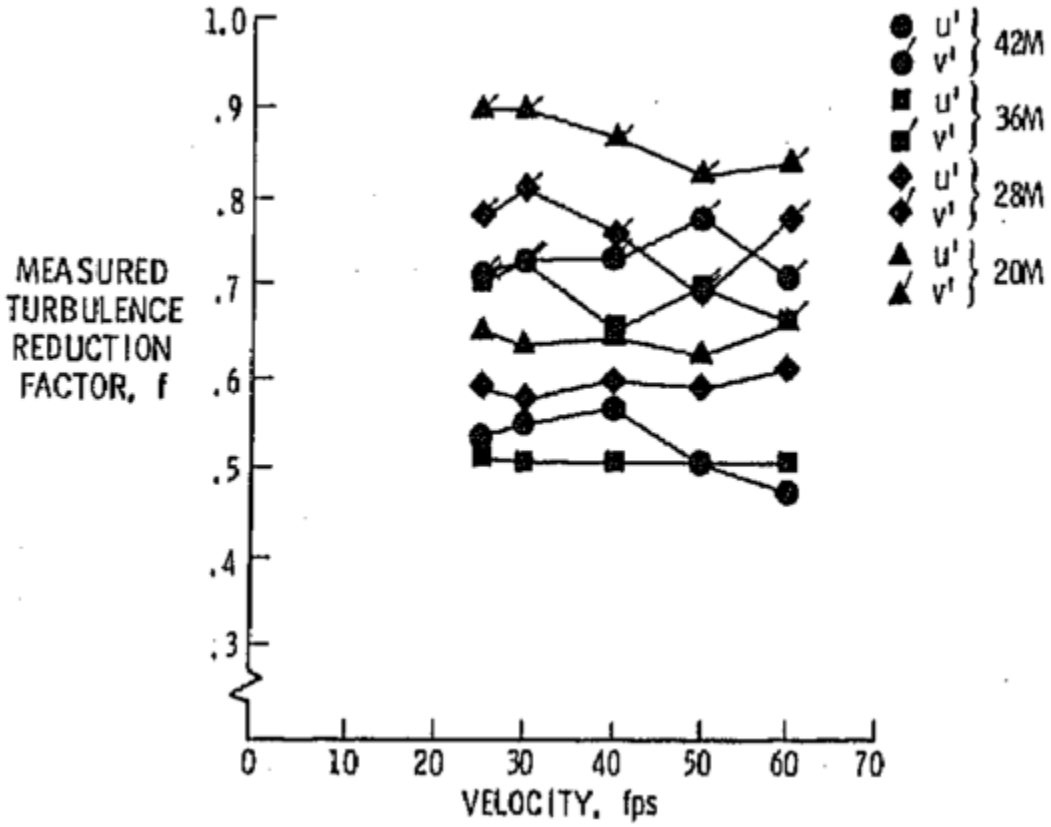

Figure 9. Turbulence reduction factors [10]

It was also found that additional screens give a lower turbulence reduction factor. Distance between screens and the screen angle have a low impact on the turbulence reduction. Furthermore, Scheiman and Brooks found that the later screens are more important than early screens. This means that initial screens can have a less dense mesh yielding a lower pressure drop and higher wind tunnel velocities. Scheiman and Brooks give the following:

- Two identical screens are better than one
- A honeycomb plus one screen is better than three screens

- A honeycomb plus two screens gave the best results

Scheiman and Brooks did not study combinations of honeycombs and screens past one honeycomb plus two screens. However, Dryden and Schubauer [11] did study higher combinations of screens and screen types. The results found are given in Table 2 below where *Iave* is the average turbulence intensity and *Ut* is the average test section flow velocity.

Table 2. Test section turbulence for different screen configurations [11]

Screen Pack Type:	*Iave/Ut*
No Screen	0.265
1-18 mesh screen	0.182
1-20 mesh screen	0.15
1-24 mesh screen	0.195
1-60 mesh screen	0.114
2-18 mesh screens	0.133
3-18 mesh screens	0.099
6 screens, 3-20 mesh, 3-24 mesh	0.043

It can be seen that while the results are not as predictable as would have been hoped, the six screen combination gives the highest turbulence reduction.

Screen spacing has a different guideline depending on which study is referenced. As previously stated, Scheiman and Brooks did not find significant differences in turbulence reduction with different screen spacing. However, Mehta [12] found that for typical wind tunnel screen mesh sizes turbulence persists for at least 200 screen mesh lengths past the screen. On average this means that the flow recovers by roughly 1.6 centimeters from the screen. Barlow et al. [7] recommends that each screen has a spacing of 30 mesh sizes or 500 wire diameters from the screen being used. In addition, Bradshaw and Mehta [8] recommend a screen spacing of 0.2 settling chamber diameters.

The above guidelines are minimum distances for the distance between screens and distances greater than the minimums will not have a significant effect on the turbulence reduction. Furthermore, the minimum distances between screens are in many cases impractical when considering the mechanisms for securing the screens.

It was decided to use one honeycomb plus six screens with 7.62 cm between each screen. Three 24 mesh screens, one 32 mesh screen, one 46 mesh screen, and one 56 mesh screen were used. These mesh sizes were based on material availability, experienced wind tunnel designer recommendations, and the desire to incrementally reduce the scale of the turbulence in the flow.

Settling Distance:

A longer settling distance follows the screen section which allows the flow to stabilize before entering the contraction section. Unstable flow entering the contraction section would cause flow separation and could propagate to the test section resulting in

additional turbulence. According to Bradshaw and Mehta the distance between the last screen and the start of the contraction section should be at least 0.2 settling chamber diameters. This distance allows the flow to stabilize and prevents the flow from distorting as it flows through the last screen. Settling distances longer than 0.2 settling chamber diameters will cause unnecessary boundary layer growth. A settling distance of 0.61 meters was used which is 0.2 multiplied by the settling chamber diameter of 3.05 meters.

Contraction Section:

The contraction section directly follows the settling chamber (honeycomb/screens/settling distance). The contraction section takes steady flow from the wind tunnel inlet cross sectional area and brings it to the test section cross sectional area. Through conservation of mass this smoothly brings the flow from a lower velocity to a higher velocity flow. It is desirable to minimize the length of the contraction section as additional length increases boundary layer growth. However, if a high contraction ratio, given below in Equation 2, is used over too short of a distance, flow separation will occur. In addition, high contraction ratios require more power from the wind tunnel fan. The ideal contraction ratio minimizing boundary layer growth and maximizing air velocity is between 6 and 9 [13]. This is largely based on trial and error as limited theoretical research has been published on contraction section shapes and sizes. Sound contraction section designs in one wind tunnel may have flow separation in another for unknown reasons.

$$Contraction\ Ratio = \frac{Inlet\ Cross\ Sectional\ Area}{Outlet\ Cross\ Sectional\ Area} \quad (2)$$

The axial cross section of the contraction is largely irrelevant as long as it is smooth and is based on an effort to limit boundary layer development and flow separation. Bradshaw and Mehta give the following guidelines

- Smoothness is more important than matching exact shapes
- Curvature should be less at the outlet than at the inlet.
- Both ends should be parallel or very near parallel to the sections they are connecting to

The contraction ratio chosen was based on the maximum inlet area allowed, 3.05 meters square, and the desired test section cross section, 1.19 m square, which gives a contraction ratio of 6.2. This is in the lower end of the recommended range but was chosen because the current wind tunnel fan is underpowered for this application. The axial contour of the contraction section is a fifth order polynomial that the manufacturer has “had good luck with recently” in several other wind tunnels.

Test Section:

The test section, or working section, is the lowest turbulence section of the wind tunnel where all testing is completed. The test section drives the size of the wind tunnel based on the type of testing desired.

To facilitate hot-wire testing on the wake behind wind turbines it was desirable to test the largest diameter wind turbine possible to match the Reynolds number of commercial wind turbines. Turbines with similar Reynolds numbers will have similar

flow characteristics. Commercial wind turbines have a Reynolds number of $6x10^6$, based on the blade cord length at 75% of the blade radius, which for a 30 to 90 cm diameter wind turbine would be unfeasible to match. For a 30 cm diameter wind turbine to match a commercial wind turbine Reynolds number, the rotational velocity would be so high that the blade tips would pass the speed of sound. Fortunately, after Reynolds numbers of 1^4 it is commonly accepted that flows are similar until compressibility become an issue.

Another consideration for the size of the test section is that it is not desirable for the wind turbine wake to intersect with the wind tunnel wall boundary layer. This would cause premature boundary layer growth and invalidate wake data. It was estimated that if no unusual boundary layer growth occurs in the contraction section, the average height of the boundary layer in the test section would be 15.24 cm.

In summary, the largest possible cross section test section was desired for this testing given the available space. It was also recommended to use polycarbonate walls for the test section as polycarbonate is impact resistant in the event of a turbine blade failure. Polycarbonate was available in 1.21mX2.42m sheets which set the test section cross section to 1.19m square and 2.42m long. A longer test section could have been designed, but additional length would have induced additional boundary layer growth. The effect of the boundary layer on the flow inside the test section is referred to as “wall effects”. Wall effects on the flow will increase the average velocity in the center of the wind tunnel through conservation of mass as the boundary layer effectively reduces

the area that the flow is going through. It was decided to keep the test section at 2.44 meters long. However, according to Bradshaw and Mehta the flow entering the test section will take 0.5 test section diameters, or 59.69 cm, until non-uniformities are reduced to an acceptable level. This reduces the working area of the test section to approximately 1.83 meters.

Diffuser:

The diffuser follows the test section and smoothly transitions the flow to the fan diameter. Flow separation in the diffuser can cause pressure fluctuations and turbulence in the test section. To prevent flow separation, the diffuser area ratio should not exceed 2.5 and the angle between the diffuser and the wind tunnel axis should not exceed five degrees.

$$Diffuser\ Area\ Ratio = \frac{Outlet\ Area}{Inlet\ Area} \quad (3)$$

The diffuser designed used an angle of 2.5 degrees and a ratio of 2.25. The diffuser is 1.22 meters square at the test section and ends as an octagon roughly matching the 1.83 meter diameter of the fan. A rubber coupling connects the diffuser to the fan and prevents fan vibrations from spreading to the rest of the wind tunnel and causing turbulence.

Fan:

The fan used was salvaged from a previous experiment, has 34 hp, and six-1.8 meter diameter blades. This is an underpowered fan for this application and also is not of an optimum design.

True wind tunnel fans have long and wide nose cones which smoothly transition the flow to the outside of the blades which are moving much faster than at the center. Ideal fan blades are airfoil shaped and not bent metal as in the current fan. The current fan loses mass flow through the center portion of the fan and also could have flow separation on the blades which could reduce efficiency and increase noise.

The wind tunnel is vibrationally isolated from the fan by a rubber coupling. In addition, the fan is resting on four vibration reducing rubber mounts connecting the fan to its stand. The stand is also resting on rubber pads which further reduce fan vibration spread to the floor.

Model Wind Turbine Design:

A 61 cm diameter wind turbine was chosen as it was the largest diameter that could fit in the wind tunnel while not interfering with the wind tunnel boundary layer. It is beneficial to have the largest diameter possible to obtain a Reynolds Number closer to that of a commercial wind turbine. Commercial wind turbines have Reynolds Numbers in the range of $1x10^6$. However, it is commonly accepted that flows at $Re=1x10^6$ and $Re=1x10^4$ have similar flows structures. The Reynolds number of the model wind turbine, based on the blade at 75 percent length at 300-500 rpm is $6x10^4$. This will yield comparable flows to commercial wind turbines.

A model wind turbine was designed and fabricated for this research. The model wind turbine chosen for this research has a 61 cm diameter and is scaled down from a commercial 20 meter diameter wind turbine. The airfoil is a NACA 4412, which is typical

for entry level wind turbines. Advanced wind turbines will have hybrid airfoils which are combinations of many different airfoil types at different locations on the blade.

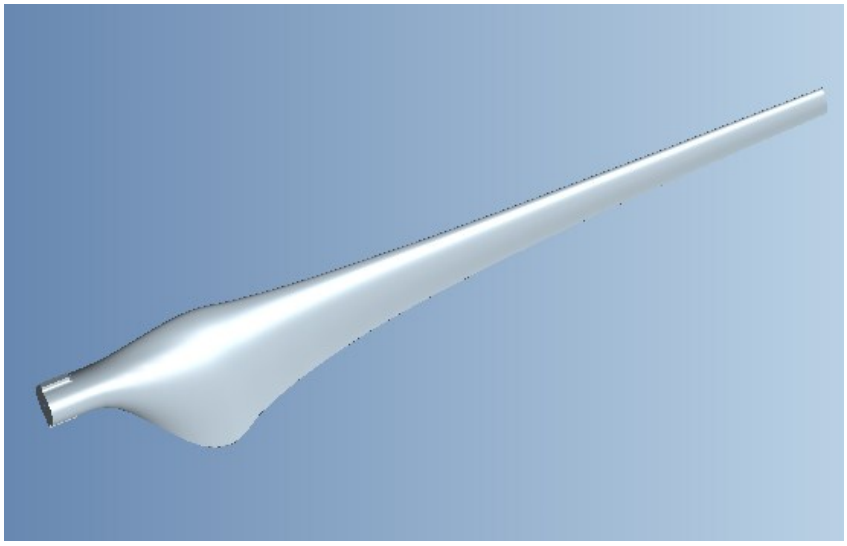

Figure 10. NACA 4412 blade used for model wind turbine.

The hub was chosen to have a cone leading edge as can be seen below in Figure 11.

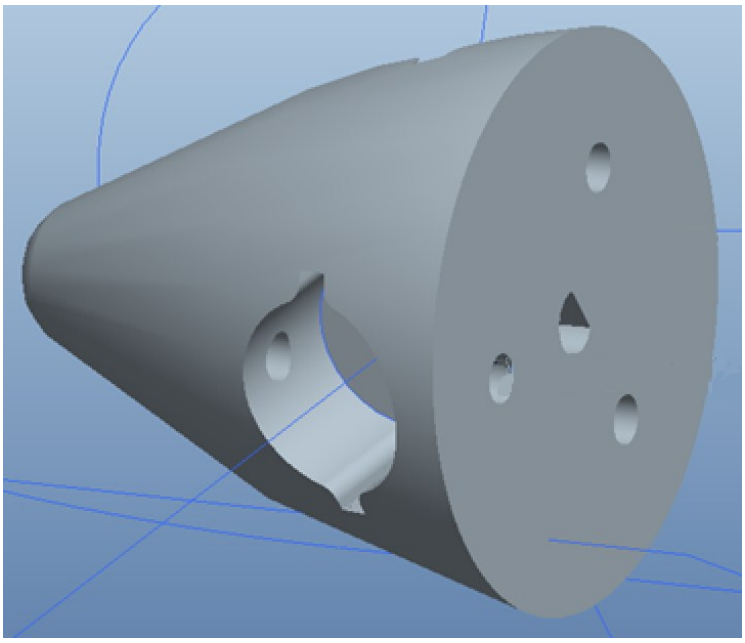

Figure 11. Model wind turbine hub

The blades can be mounted in two positions on the hub. One position allows the blades to rotate clockwise so the motor can drive the rotational velocity. This functionality was not used for this experiment. The second position allows the blades to spin the opposite direction driving the DC brushless motor allowing for basic power estimation. A set pin holds the blades in place.

Figure 12. Model wind turbine DC brushless motor

The body is comprised of a DC brushless motor shown above in Figure 12. The motor is capable of controlling the rotational velocity of the wind turbine and includes Hall Effect sensors to measure turbine rotational velocity.

Figure 13. Completed model wind turbine

Turbulence Measurement Apparatus Design:

Turbulence was measured with a 2D X-type miniature hot wire anemometer. This type of anemometer assumes the flow is two dimensional and that the flow stays within 45 degrees of the probe axis. No flow reversal can occur. This type of anemometer is adequate for this testing as macro flow structures are being observed and small eddies and eddy dissipation is not a concern. A fixture was fabricated to attach the hot wire to the traverse. As can be seen in Figure 14, the mounting fixture holds the hot wire out in front of any turbulence caused by the fixture or the traverse.

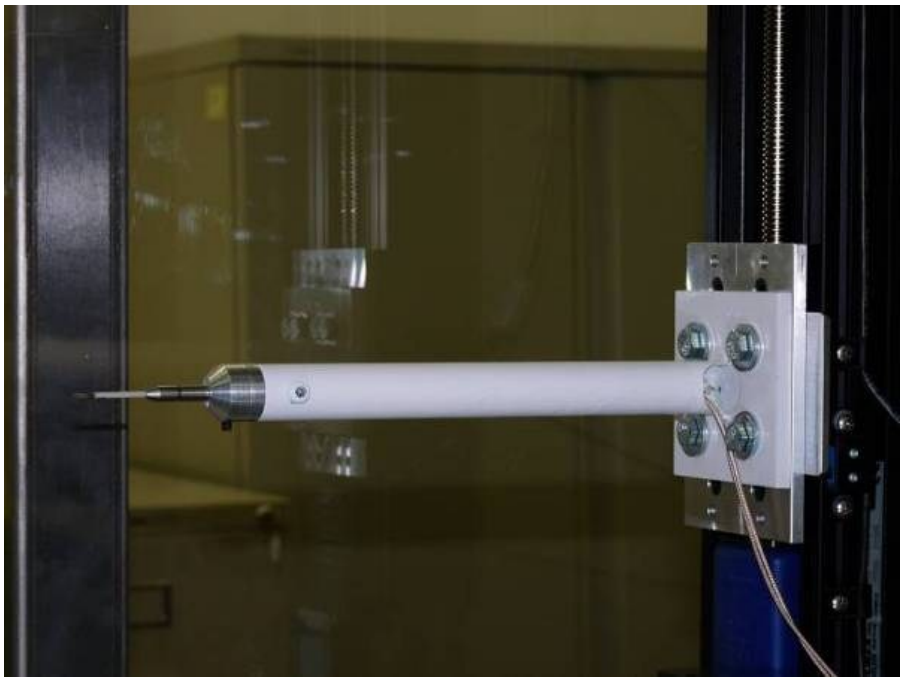

Figure 14. Hot wire mounting fixture

Calibration was completed in the Armfield C-18 wind tunnel at the University of Wisconsin Milwaukee. The C-18 has a 15.24 cm square cross section, and measures velocities with a pitot tube up to 40 m/s. The calibration apparatus is shown below in Figure 15.

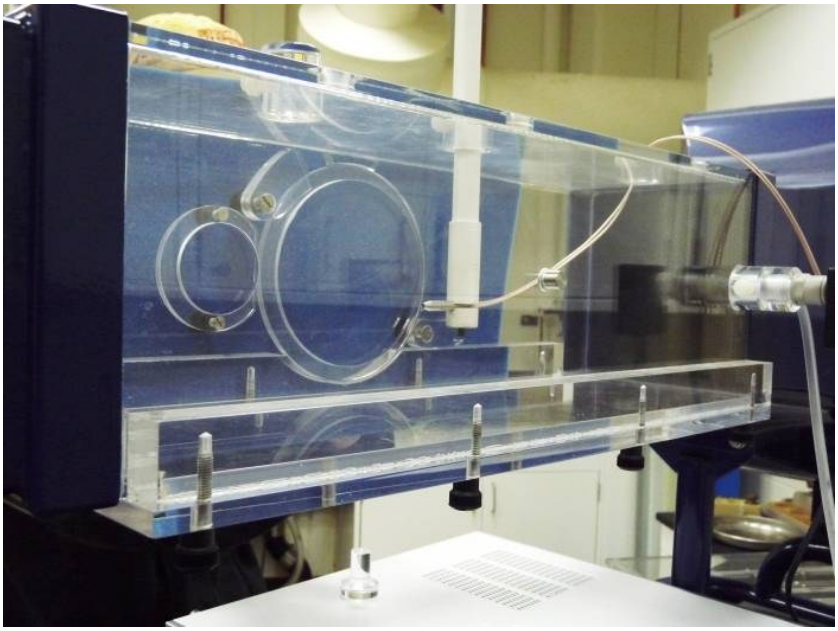

Figure 15. Armfield C18 wind tunnel used for hot wire calibration

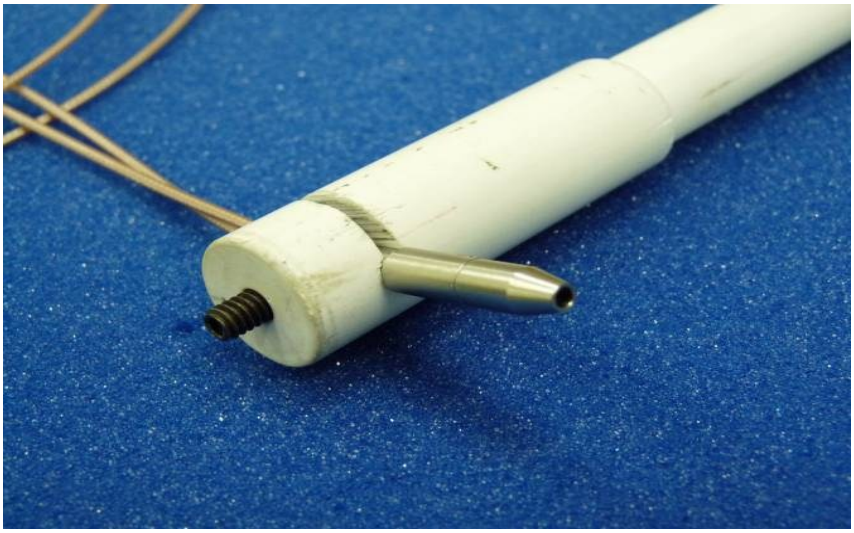

Figure 16. Hot wire calibration fixture

Measurement Automation:

To enable the positioning of the hot wire anemometer, a custom built three axis traverse was built and installed in the wind tunnel. This enables a grid of measurements to be accurately and repeatedly taken. Control was performed through LabVIEW 2012.

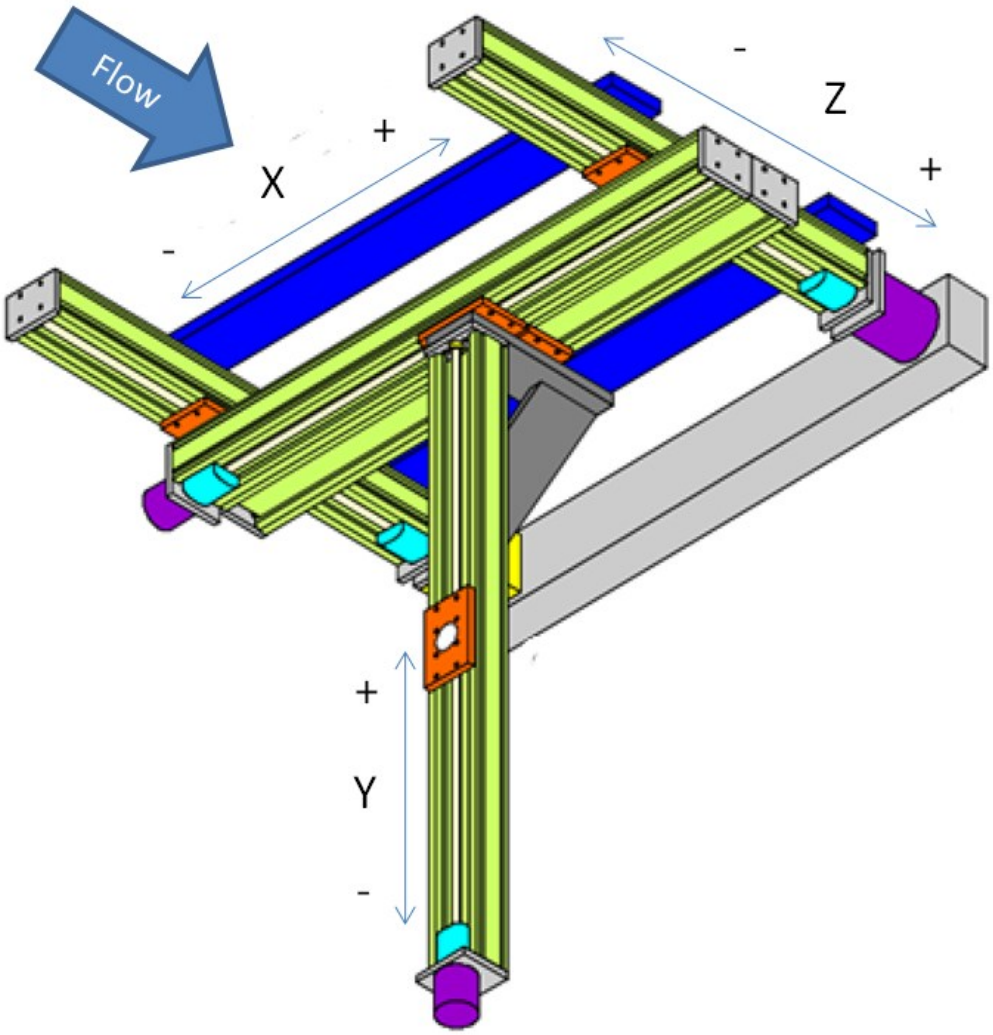

Figure 17. Model of 3-axis traverse used in wind tunnel

Data Acquisition:

Data acquisition and traverse control was programmed in LabVIEW. LabVIEW is a visual programming language which allows the user to eliminate text commands and to manipulate the program graphically. The "VIEW" in LabVIEW stands for Laboratory Virtual Instrumentation Engineering Workbench.

The LabVIEW program allows for the user to obtain data for either a series of horizontal or vertical grids. Each grid is comprised of a user defined number of points where the

hotwire stops moving, takes a user defined number of samples, and saves the average velocity and standard deviation of the velocity to a spreadsheet format.

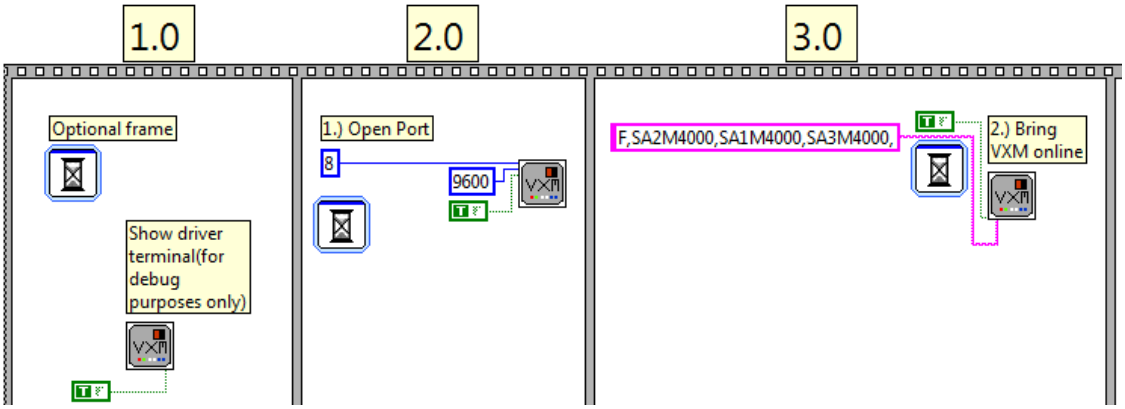

Figure 18. Wind Tunnel Code Initialization

LabVIEW runs in parallel unlike most traditional programing languages that run in series. This presents an issue when events need to occur in a specific order. Above, in Figure 18, can be seen three frames in a flat sequence structure. Programing inside each frame runs in parallel while the frames run in sequence once the previous frame has completely finished its program.

Frames 1 and 2 prepare the computer to communicate with the traverse controller. Frame three changes the traverse controller from manual to computer control and sets the motor speeds in revolutions per minute. The motor speeds were determined through trial and error. The maximum motor speed is 6000 rpm. This was gradually reduced due to the motor stalling. 4000 rpm was the speed at which no stalling has occurred.

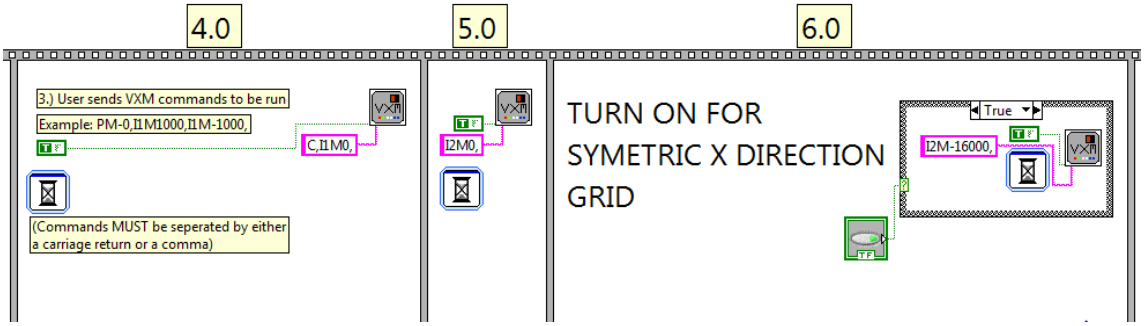

Figure 19. Wind Tunnel Code Initialization and Symmetric X Direction Setup

To ensure that the traverse always starts in the same position, frames 4 and 5 bring the traverse to its limits in one corner of the test section of the wind tunnel. The horizontal component of the traverse perpendicular to the flow has a motor on the end of it as can be seen in Figure 19. This means that the hotwire can get closer to one wall than the other. If the green button in frame 6 is false, nothing happens and the hotwire is left in the corner. However, if the button is true, the hotwire moves out such that the starting and ending point of the hotwire are centered in the test section.

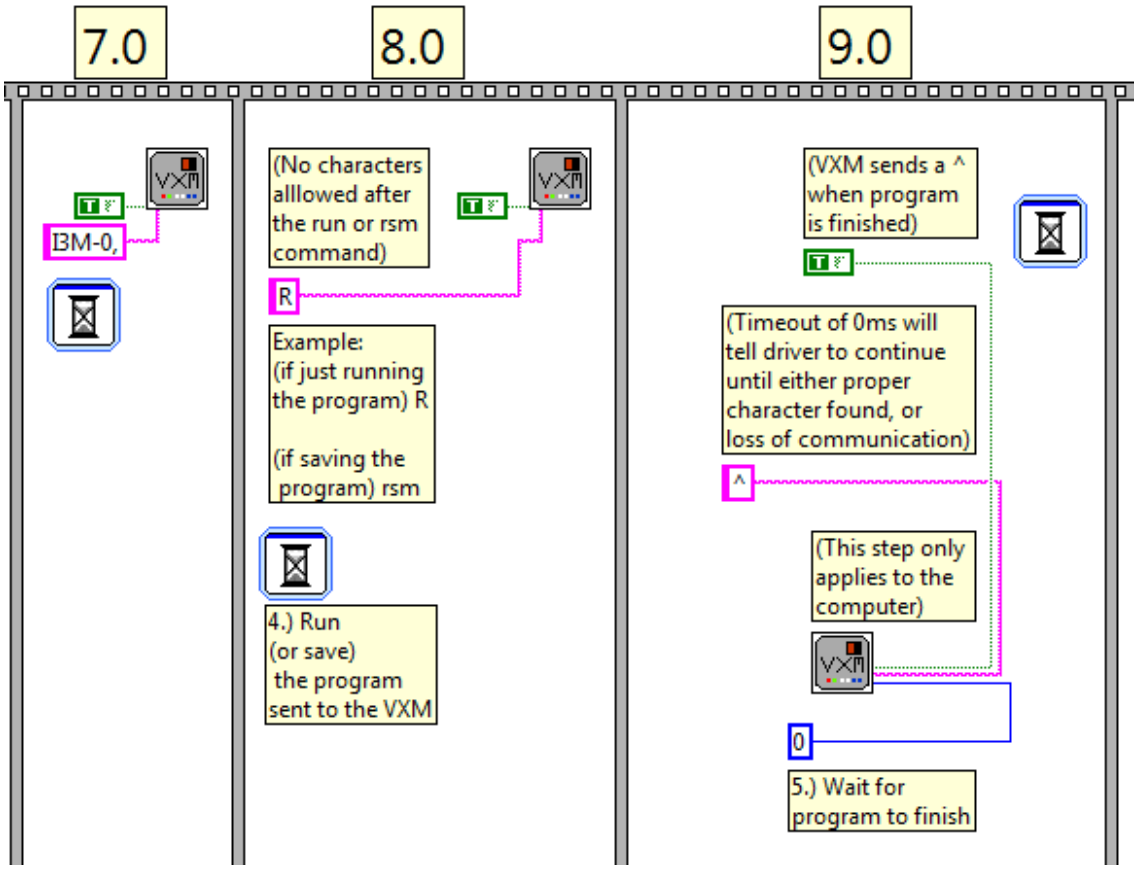

Figure 20. Run traverse code and wait for completion

Frame seven sends the code to move the traverse to the bottom of the wind tunnel. Frame eight sends the command to the traverse controller to execute the code developed in frames four, five, six, and seven. Frame nine waits for the traverse controller to return a "^" to indicate that the traverse has completed its motion. This signals to LabVEIW that it can move the next frame in the flat sequence.

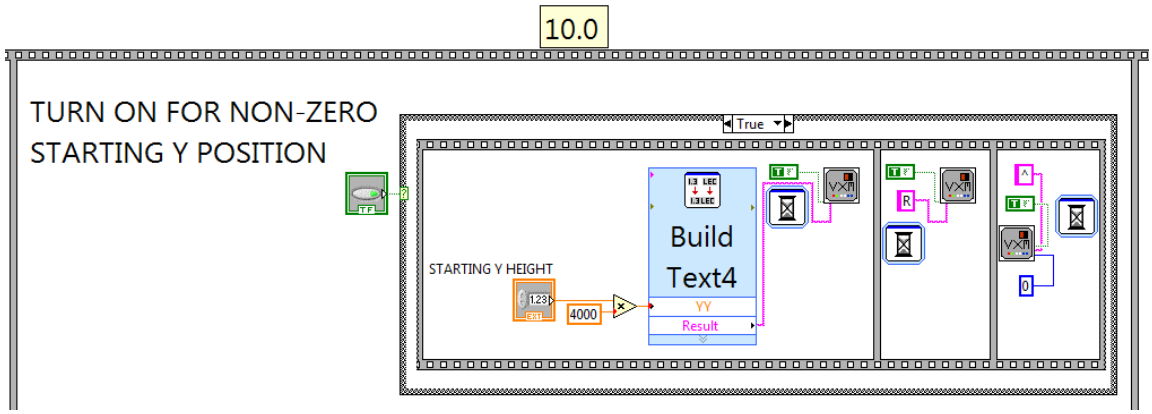

Figure 21. Set non-zero starting position

To enable the user to move the starting point up or down, frame ten allows the user to input the distance above the bottom of the test section that the hotwire should start. As can be seen above in Figure 21, the starting height is multiplied by 4000 as 4000 revolutions will move the hotwire 2.54 cm.

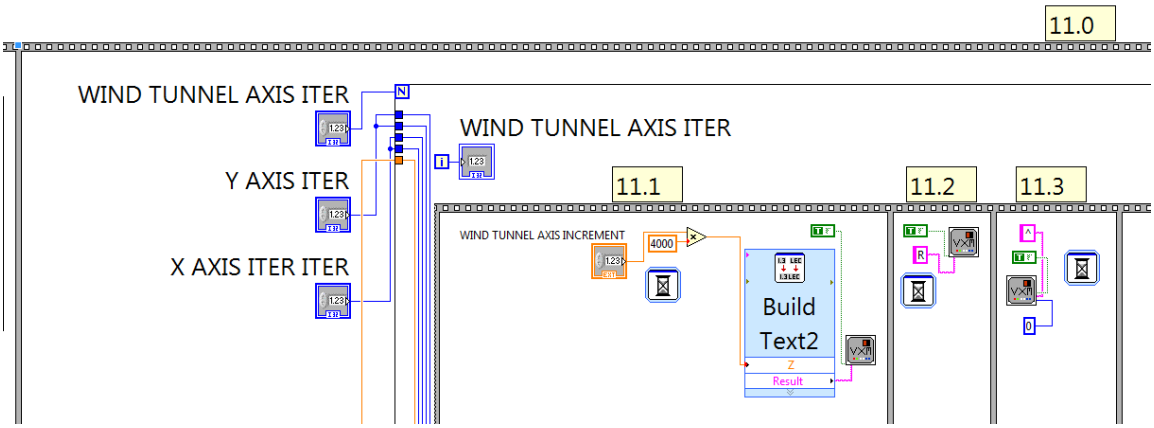

Figure 22. Set number of iterations

Frame eleven is a large frame which contains the traverse movement and data acquisition. It will be divided up into several screen shots. The box containing the inner flat sequence is a for-loop which allows the user to choose how many vertical planes of data will be taken perpendicular to the flow. Frame 11.1-11.3 set the starting location for these planes.

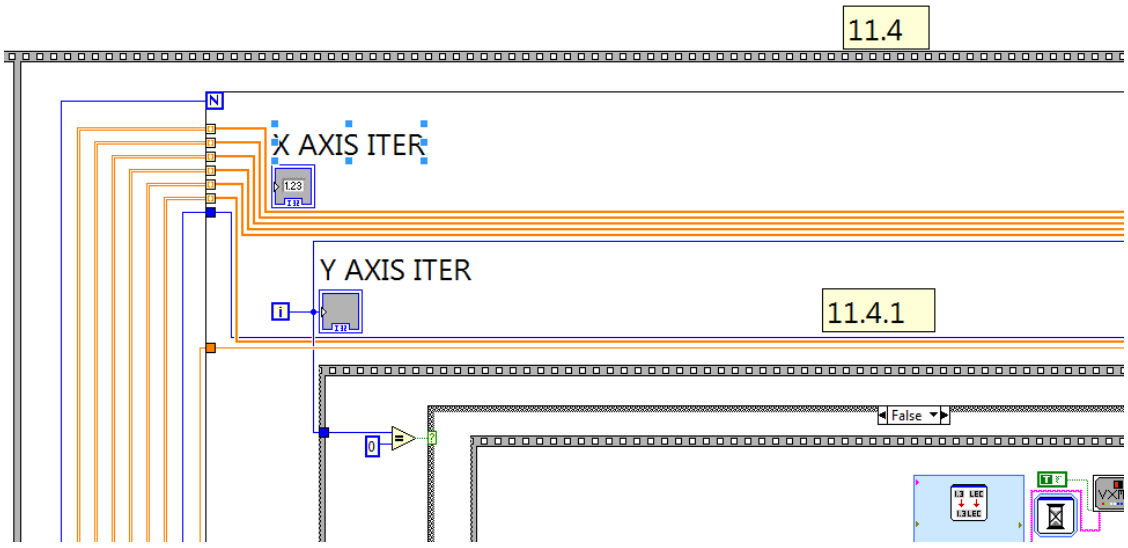

Figure 23. X and Y axis for-loops

Frame 11.4 contains two for-loops which set the number of rows and columns in each plane. These for-loops also drive the data acquisition as will be seen below.

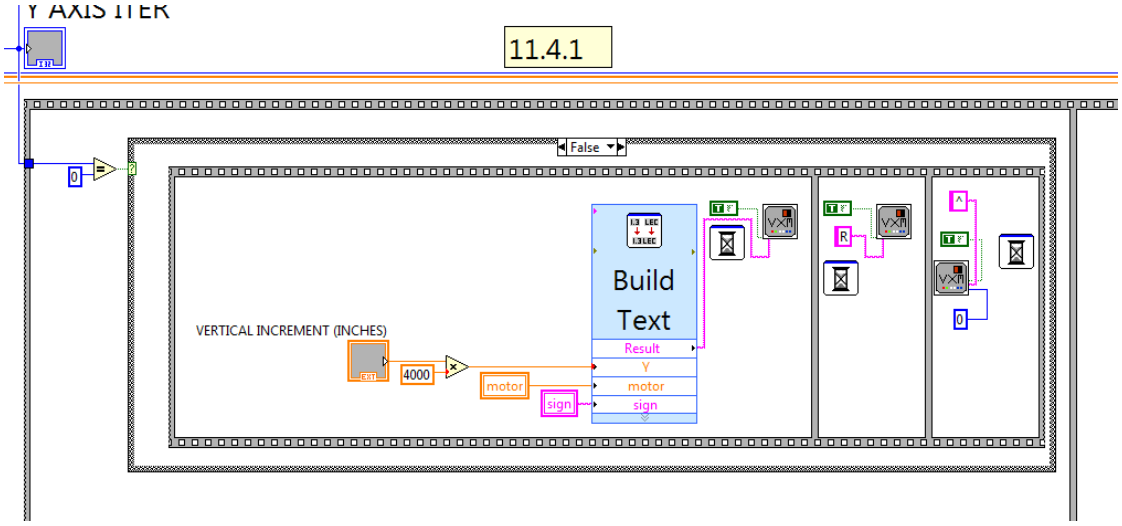

Figure 24. Set Y axis increment

Frame 11.4.1 moves the hotwire in the vertical Y axis. When the number of Y axis iterations of the for-loop equals 0, the true path of this case structure is followed and nothing happens. For all other iterations the traverse is moved up by a user defined distance.

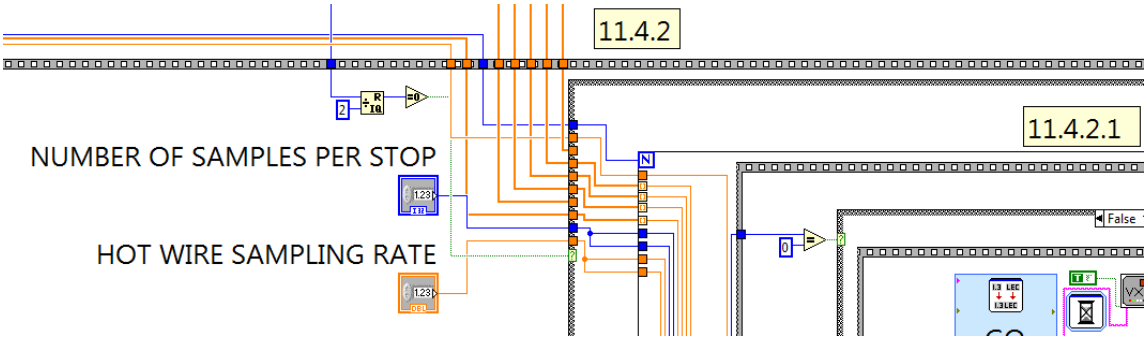

Figure 25. Set number of samples and sampling rate

Frame 11.4.2 contains the horizontal for loop which moves the hotwire either direction in the X axis depending on if it is in an even or odd Y axis iteration. This enables the hotwire to take data every time it moves across the wind tunnel. It will move to one wall while taking data, move up, move to the other wall while taking data, move up, etc. Every other row will have data recorded in a different order than the row before it (i.e. the point above the first position in row number one will be the last position in row number two). A MATLAB code discussed later in this paper addresses this issue and reverses the order of the data in every other row.

Frame 11.4.2 also allows the user to set the number of samples the hotwire will take per data point that it saves and allows the user to set the sampling rate.

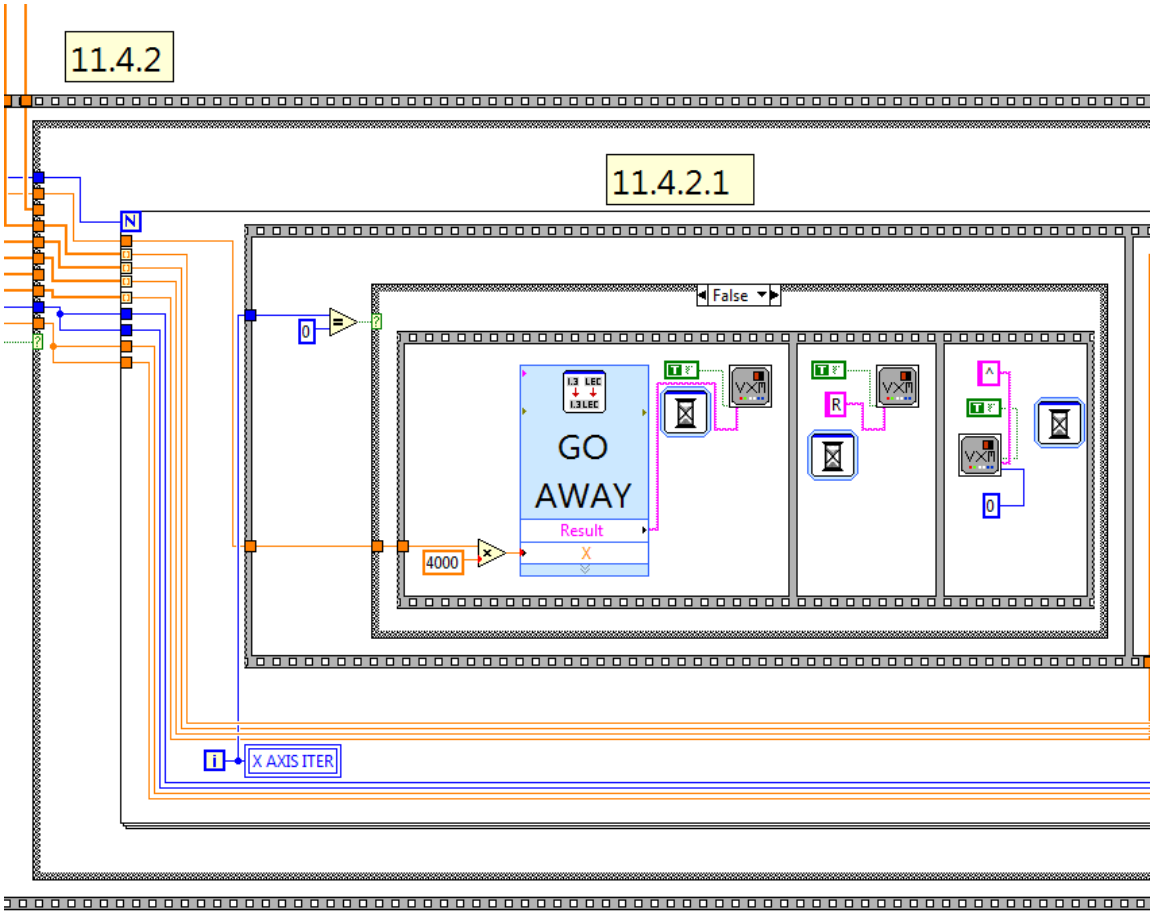

Figure 26. X axis hotwire movement

Frame 11.4.2.1 moves the hotwire away from the user (presumably on the door side of the wind tunnel) in the negative X direction on odd Y axis iterations.

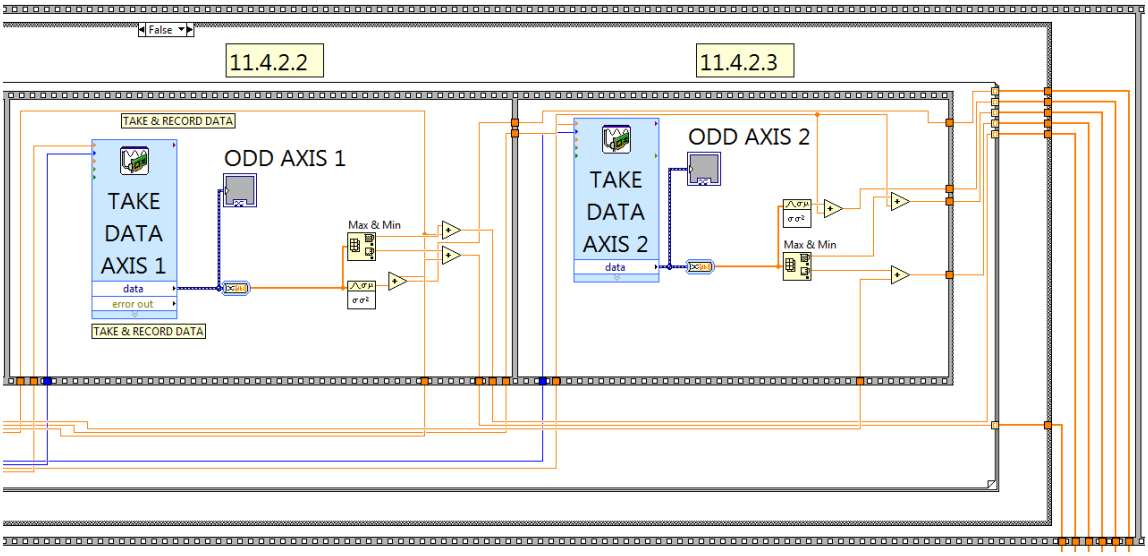

Figure 27. Data acquisition

Frames 11.4.2 and 11.4.3 record the maximum, minimum, and average hotwire velocity for the user defined number of samples at each hotwire sampling point. Hardware limitations prevent taking data from both hotwire axis at the same time. A high number of samples are recommended to eliminate discrepancies due to lag between data on hotwire axis 1 and 2.

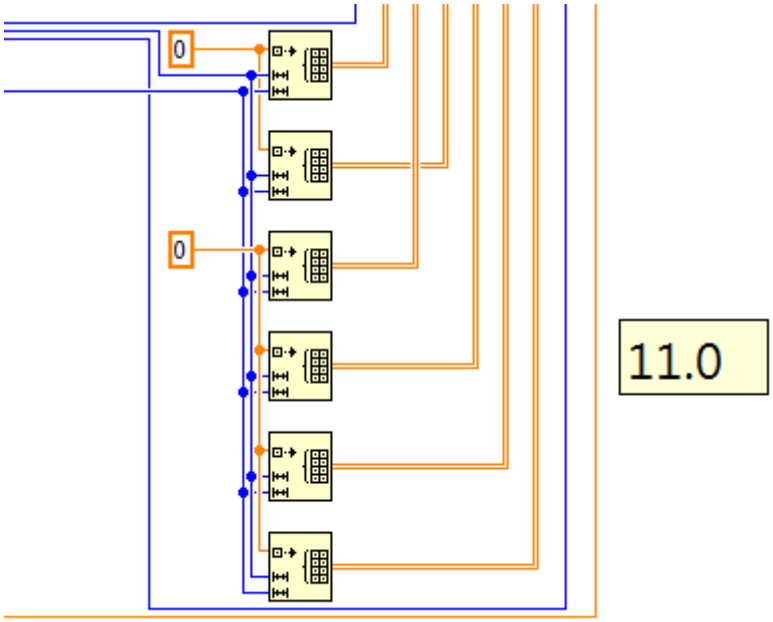

Figure 28. Initialize array and save data

LabVIEW auto indexes the data as the orange data lines leave the X and Y for-loops. Frame 11.0, above, also initializes six 2-dimensional arrays and saves the max, min, and average velocity data for each hotwire axis

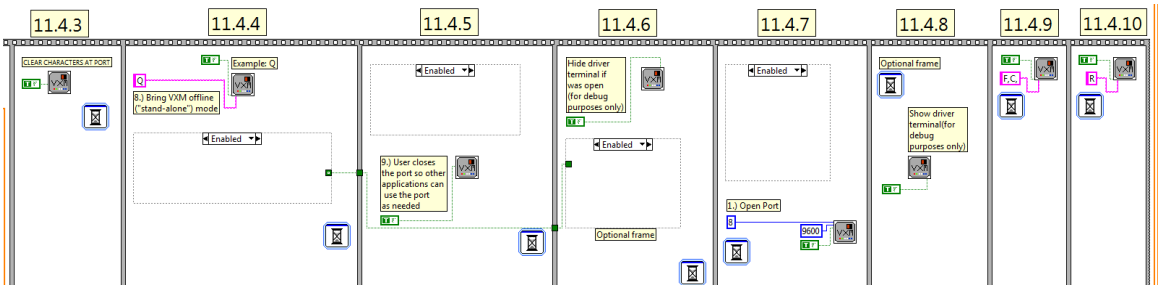

Figure 29. Reset traverse controller

Between each Y axis iteration, frames 11.4.3 through 11.4.10 clear, close, and restart the traverse controller. This was found to be necessary to prevent the controller's buffer from filling and causing the LabVIEW program to freeze.

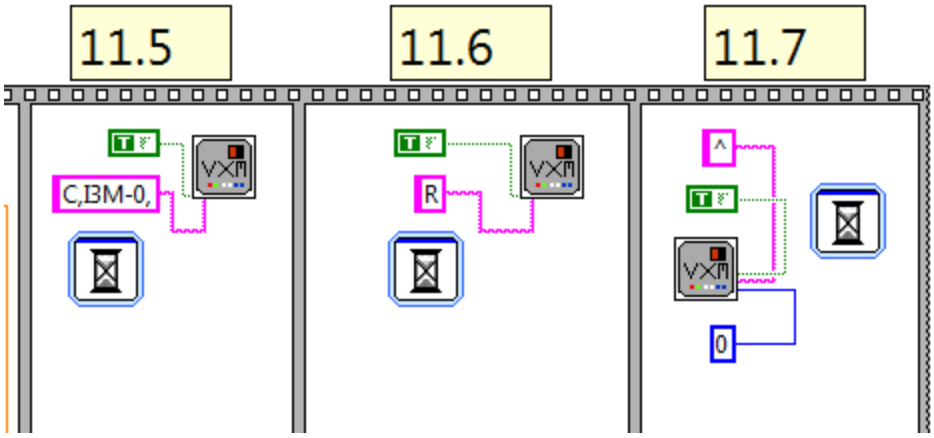

Figure 30. Return hotwire to starting position

Frames 11.5 through 11.7 return motor 3 to its starting position.

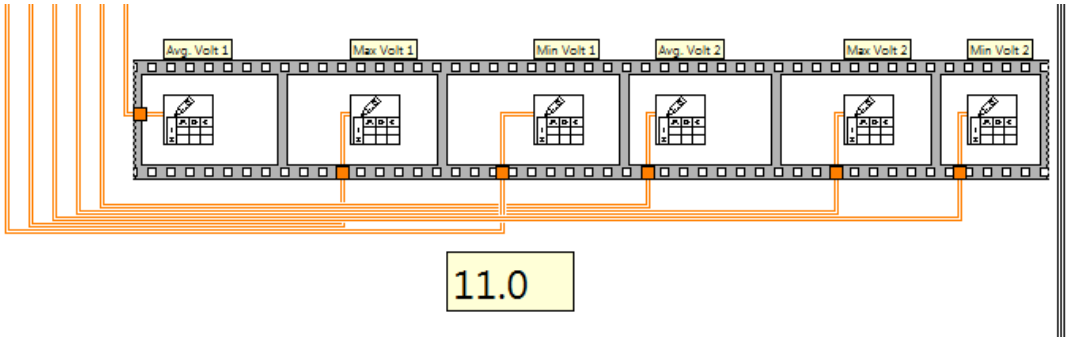

Figure 31. Export data to Excel

Once the data acquisition is complete the arrays from Figure 31 are saved in Excel format. The user is prompted for the file name and location.

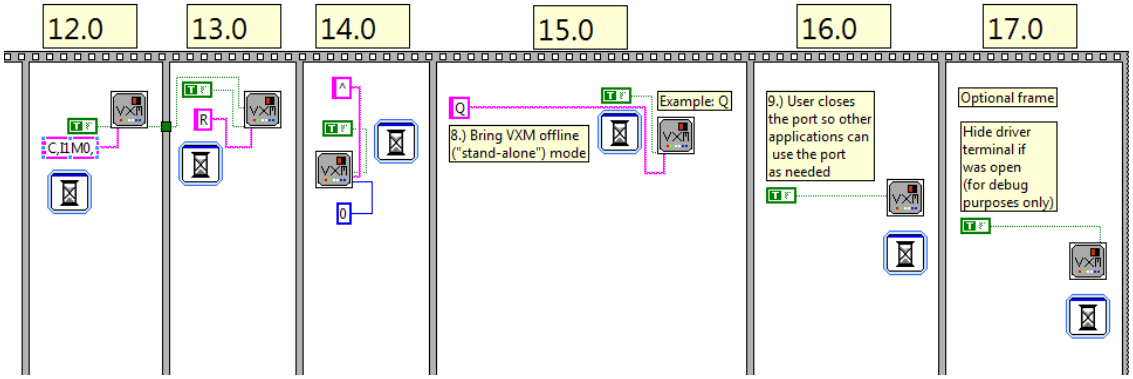

Figure 32. Reset and stop wind tunnel program

Frames 12.0 through 17.0 return the hotwire to the remaining starting positions and close the traverse controller.

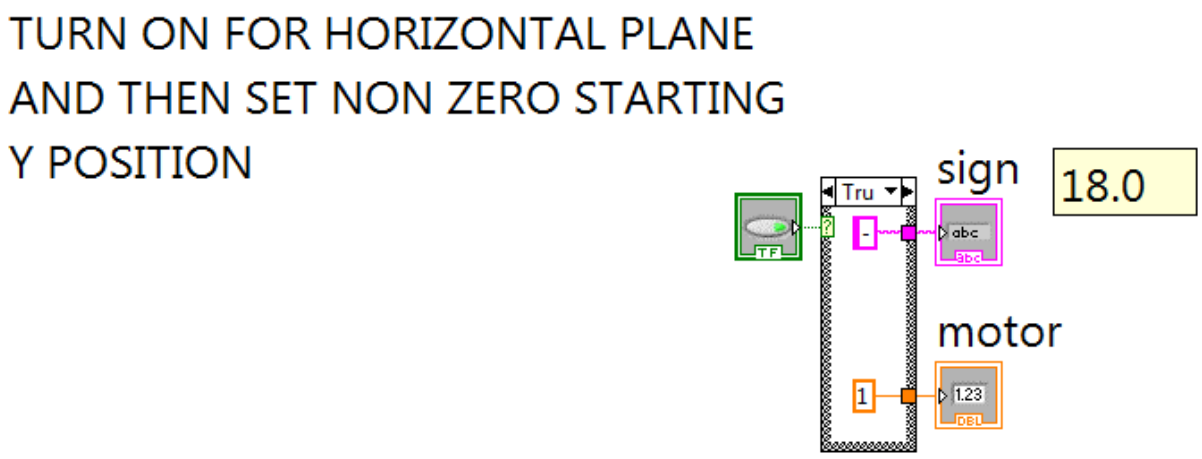

Figure 33. Set vertical or horizontal data plane

Section 18.0 is outside of the main flat sequence structure and determines if a horizontal or vertical plane of data will be acquired. If the button above is true, the sign and motor of the Y axis changes such that it is now the Z axis.

For continuity, zoomed out screen shots of the wind tunnel LabVIEW program are given below.

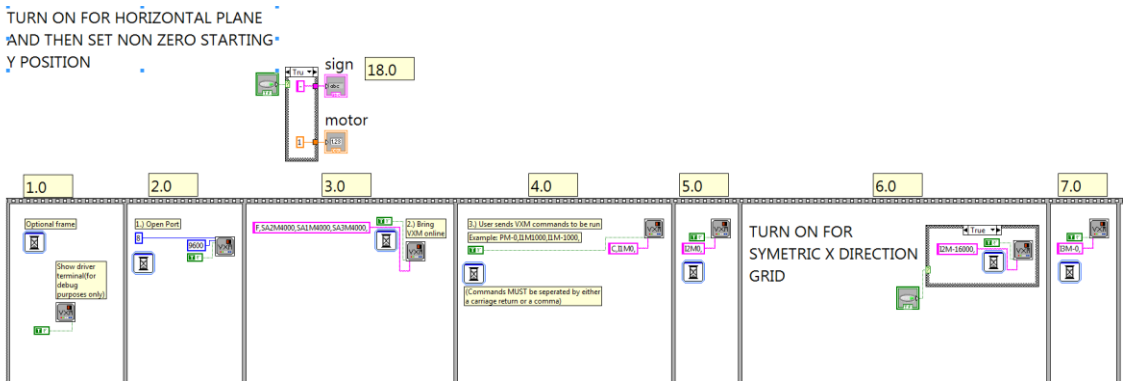

Figure 34. Frames 1 through 7.0 and 18.0

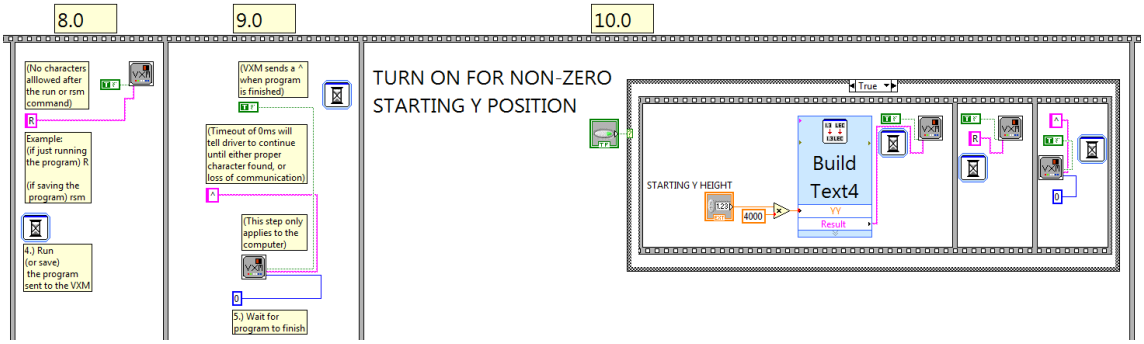

Figure 35. Frames 8.0 through 10.0

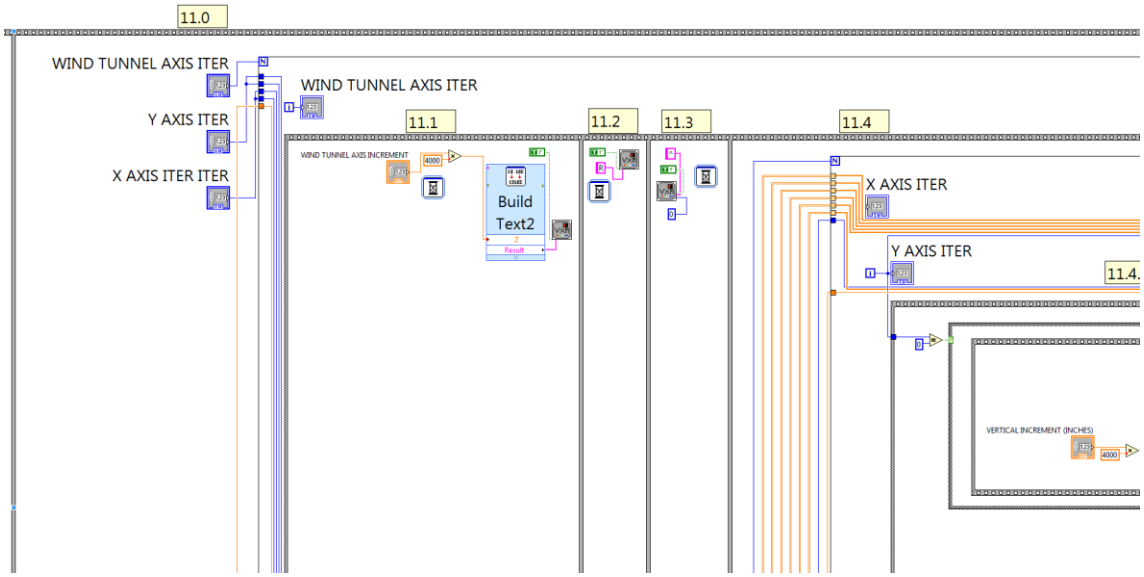

Figure 36. Frame 11.1 through 11.4

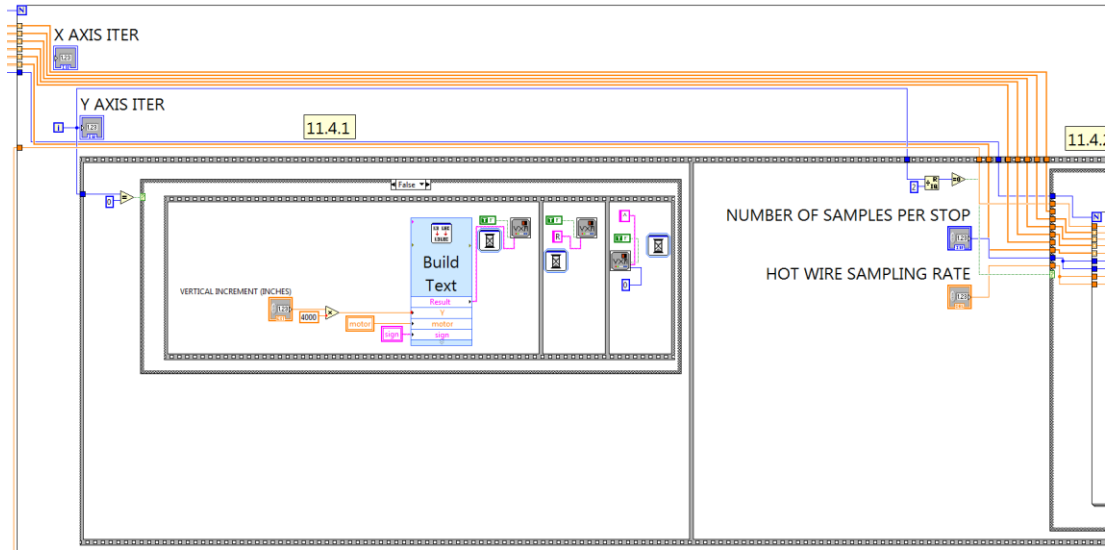

Figure 37. Frame 11.4.1

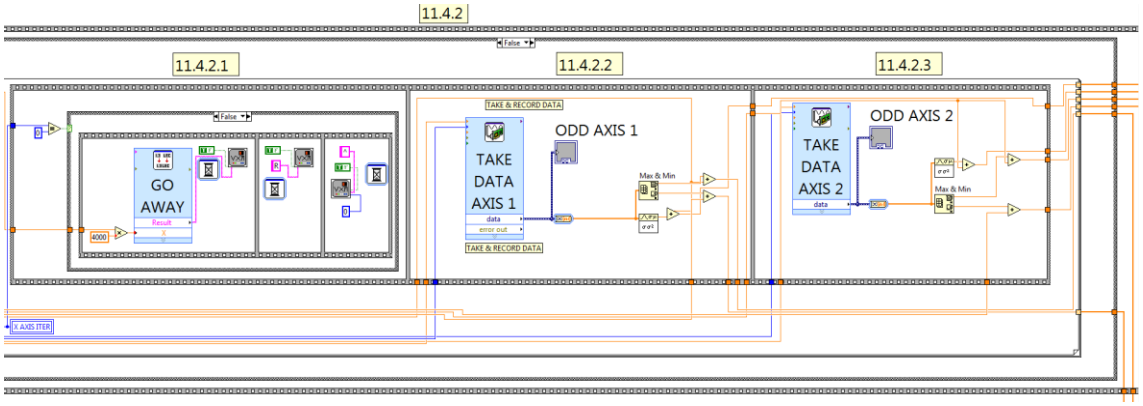

Figure 38. Frame 11.4.2.1 through 11.4.2.3

A MATLAB program was created to read in the spreadsheet, convert the data to a matrix corresponding to wind tunnel position, and convert the data from the hot wire anemometer axis to the wind tunnel axis. The converted data was then graphed in MATLAB.

The following is the MATLAB code used to convert the hotwire voltages to velocity. WindTurbine is the main function that calls the rest of the .m files used.

```
function
[dummy,postS1mean,postS1meanConv,VTurbIntent,UTurbIntent,Umean,Udev,Vmean,Vdev]=WindTurbin
e()
[preS1mean, text, alldata] = xlsread('1');
[preS1dev, text, alldata] = xlsread('2');
[preS2mean, text, alldata] = xlsread('3');
[preS2dev, text, alldata] = xlsread('4');
X=size(preS1mean,1);                          %rows
Y=size(preS1mean,2);                          %collumns
postS1mean=reOrder(X,Y,preS1mean);            %reorders the matrix
postS1dev=reOrder(X,Y,preS1dev);
postS2mean=reOrder(X,Y,preS2mean);
postS2dev=reOrder(X,Y,preS2dev);
postS1meanConv=convert1(postS1mean);          %converts from voltage to velocity
Udev=postS1dev;                               %postS1meanConv./postS1mean.*postS1dev;
postS2meanConv=convert2(postS2mean);
Vdev=postS2dev;                               %postS2meanConv./postS2dev.*postS2dev;
U1mean=ConvertToU1(postS1meanConv,postS2meanConv);  %converts to sensor coordinate system
U2mean=ConvertToU2(postS1meanConv,postS2meanConv);
Umean=ConvertToU(U1mean,U2mean);   %converts to wind tunnel coordinate system
Vmean=ConvertToV(U1mean,U2mean);
contourf(Umean,10)
```

```
VTurbIntent=Udev/Umean;                    %finds turbulance intensity
UTurbIntent=Vdev/Vmean;
dummy=1;
```

Function reOrder reverses the data in every other row so that all the data is in the correct order in the matrices. For example, assume the following is a 4 X 4 grid of data points in the wind tunnel.

1 2 3 4
1 2 3 4
1 2 3 4
1 2 3 4

The LabVIEW program records the voltages in arrays in the following order:

4 3 2 1
1 2 3 4
4 3 2 1
1 2 3 4

The reOrder function matches up the data points with their physical location relative to the previous row's data.

```
function [post]=reOrder(X,Y,pre)
for N=1:X
   if mod(N,2)==1
      for i=1:Y
         post(N,i)=pre(N,i);
      end
   else
      for j=1:Y
         k=Y+1-j;
         post(N,j)=pre(N,k);
      end
   end
end
post;
```

Convert1 and Convert2 convert the voltage to a velocity using the 6^{th} order polynomial determined during calibration.

```
function [velocity] = convert1( V )
velocity=41.23*V.^6-323.35*V.^5+877.95*V.^4-635.72*V.^3-1201.6*V.^2+2349.7*V-1133.9;

function [velocity] = convert2( V )
velocity=41.23*V.^6-323.35*V.^5+877.95*V.^4-635.72*V.^3-1201.6*V.^2+2349.7*V-1133.9;
```

ConvertToU1 and ConvertToU2 converts the data to the sensor coordinate system.

```
function [VelocityInSensorCoordinateSystem]=ConvertToU1(UcalS1,UcalS2)
k1=.04; %This value is already squared
k2=.04;
VelocityInSensorCoordinateSystem=(sqrt(2)/2)*((1+k2)*UcalS2.^2.-k2*UcalS1.^2).^(1/2);

function [VelocityInSensorCoordinateSystem]=ConvertToU2(UcalS1,UcalS2)
k1=.04;
k2=.04;
VelocityInSensorCoordinateSystem=(sqrt(2)/2)*((1+k1)*UcalS1.^2.-k1*UcalS2.^2).^(1/2);
```

The constants k1 and k2 are determined during calibration if using a 2-axis calibrator. A two axis calibrator was not available so the factory recommended 0.04 was assumed. ConvertToV and ConvertToU convert the velocities from the hotwire coordinate system to the wind tunnel coordinate system.

```
function [finalConvert]=ConvertToU(U1,U2)
finalConvert=(sqrt(2)/2)*(U1)+(sqrt(2)/2)*(U2);

function [finalConvert]=ConvertToV(U1,U2)
finalConvert=sqrt(2)/2*U1-sqrt(2)/2*U2;
```

Uncertainty Analysis:

The following uncertainties given in Table 3 were produced in the Dantec miniature hotwire anemometer documentation [14]. Since small eddy dissipation was not being measured, high frequency noise from the anemometer can be neglected.

Table 3. Uncertainty Analysis [14]

Source of Uncertainty	Estimated Uncertainty %
Calibrator	2%
Polynomial Fit	1%
Probe Positioning	Negligible
Temperature Variation	1.50%
Ambient Pressure	1%
Humidity	Negligible
Total	5.50%

The uncertainty estimates above are worst case values. Temperature and pressure variation are greatly reduced due to the ability to cut off the air supply to the room during testing. In addition, a directional calibrator should be used in future testing to reduce both the calibrator uncertainty and the polynomial curve fitting uncertainty. The uncertainty for this experiment is between 3 and 5.5 percent.

Experimental Results:

Due to a long term hot wire calibration hardware issue, an earlier hot wire calibration was used. The following results are qualitative and velocities are approximate. All experiments were conducted at approximately 9 meters/second and at a wind turbine rpm of 2400 rpm.

In addition, only the wind tunnel axis hot wire had a previous calibration close enough to the current hot wire to yield reasonable results. The following discussion will be framed in terms of velocity gradients as it is well established that they are the primary drivers of turbulence.

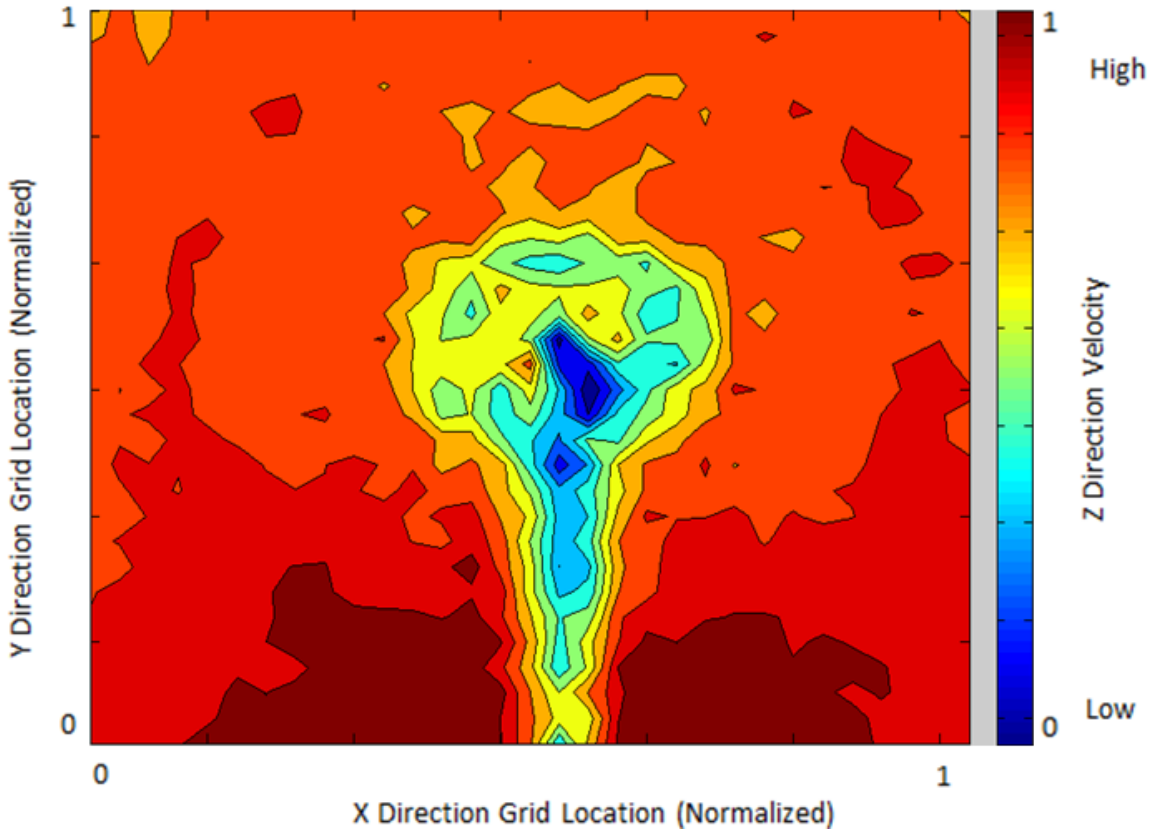

Figure 39. 78.74cm by 76.2cm grid of average wind tunnel axis velocity 15.24 cm behind the wind turbine taken every 2.54 cm.

As can be seen above in Figure 39, in the near wake, 15.24 cm behind the turbine plane, the velocity gradients are very steep and compact. This is very similar to theory and **Error! Reference source not found.** where there is a bell shaped curve of high turbulence at the center and then two more turbulence peaks at the blade tips before the flow returns to ambient.

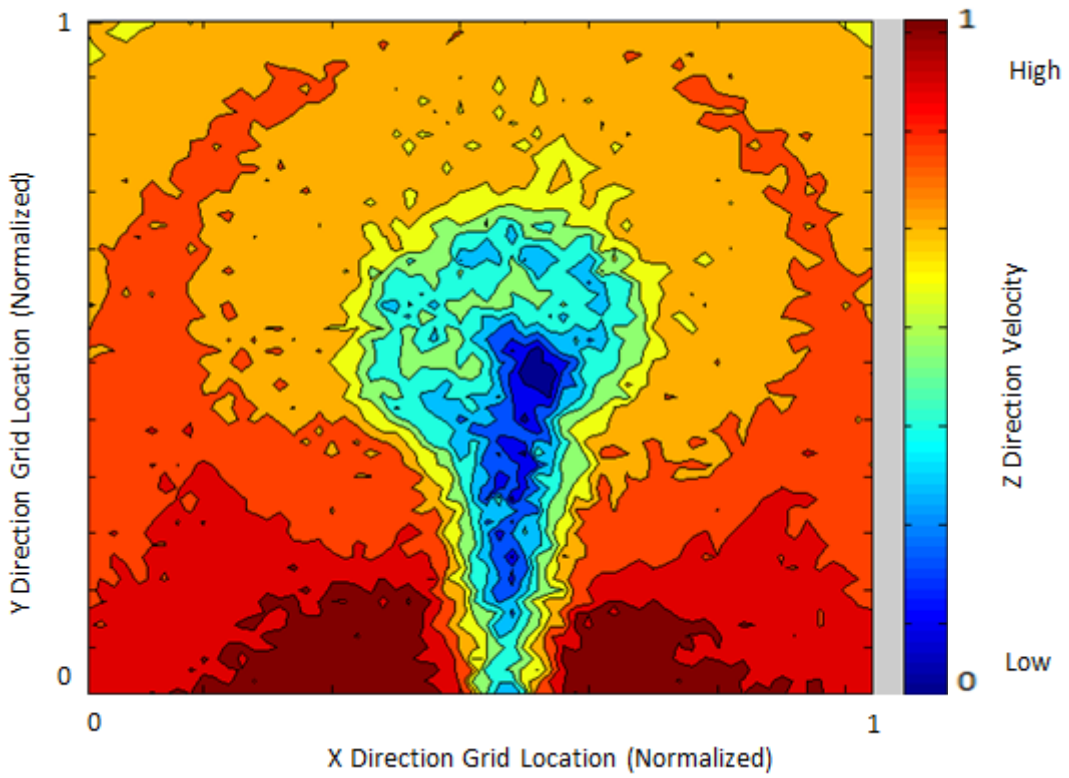

Figure 40. 78.74cm by 76.2cm grid of average wind tunnel axis velocity 30.48 cm behind the wind turbine taken every 1.27 cm.

At 30.48 cm behind the turbine plane, which is still in the near wake region, the flow structures start to become less compact as the turbulence expands. It is of interest to note how large of an effect the support tube holding the wind turbine has on the flow structure compared to above the wind turbine.

Again, Figure 40 shows a large region with a steep velocity deficit directly behind the blades with the lowest velocities behind the hub. In addition, a ring of accelerated air can be seen near the blade tips indicative of the opposing turbulence peaks in **Error! Reference source not found.** caused by the blade tips and the velocity deficit between ambient and the air flowing through the turbine.

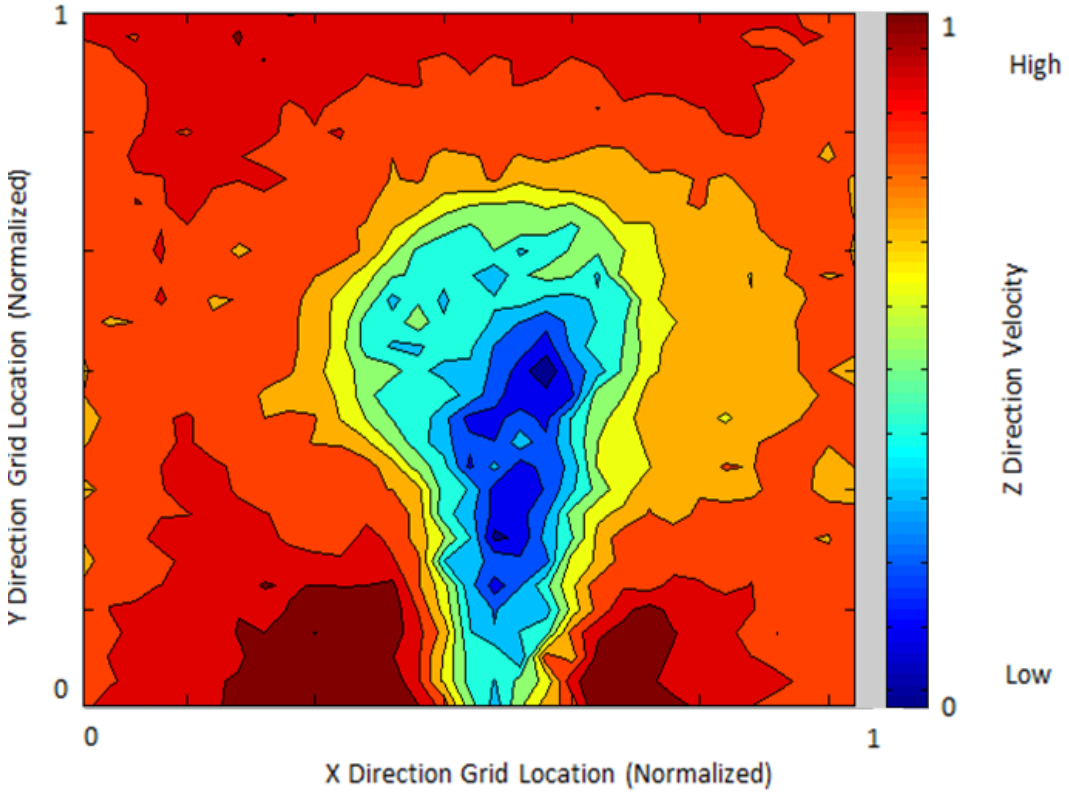

Figure 41. 78.74cm by 76.2cm grid of average wind tunnel axis velocity 60.96 cm behind the wind turbine taken every 2.54 cm.

At 60.96cm behind the turbine plane more dramatic mixing can be seen. The velocity gradients are collapsing in toward the center and transitioning to a single bell shaped curve as seen in Figure 2. Note the high velocity section on the right that is capturing the turbulence spreading from the blade tip turbulence to the center wind turbine turbulence.

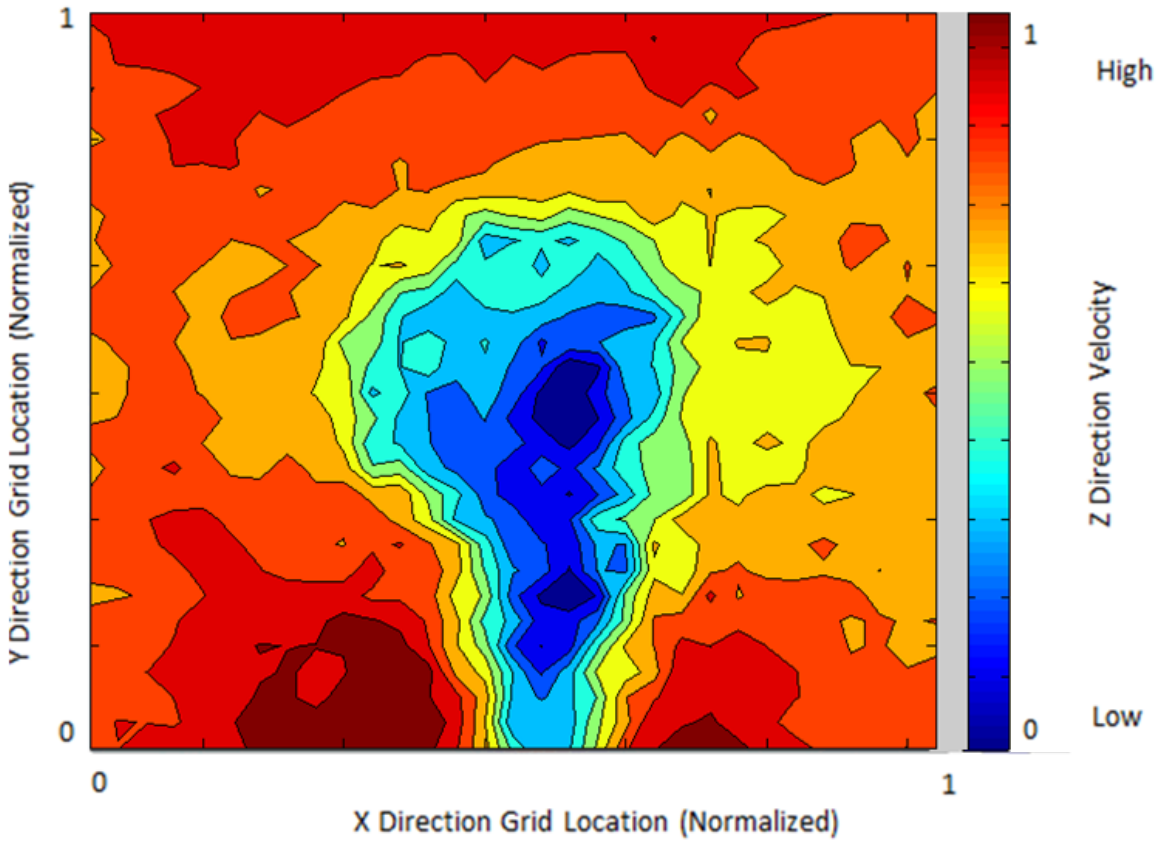

Figure 42. 78.74 cm by 76.2 cm grid of average wind tunnel axis velocity 91.44 cm behind the wind turbine taken every 2.54 cm.

Again, at 91.44 cm behind the wind turbine plane, it can be seen that the higher velocity gradients are breaking down and diffusing outward. It is also interesting that the turbulence on the right has expanded and connected to the wind tunnel wall.

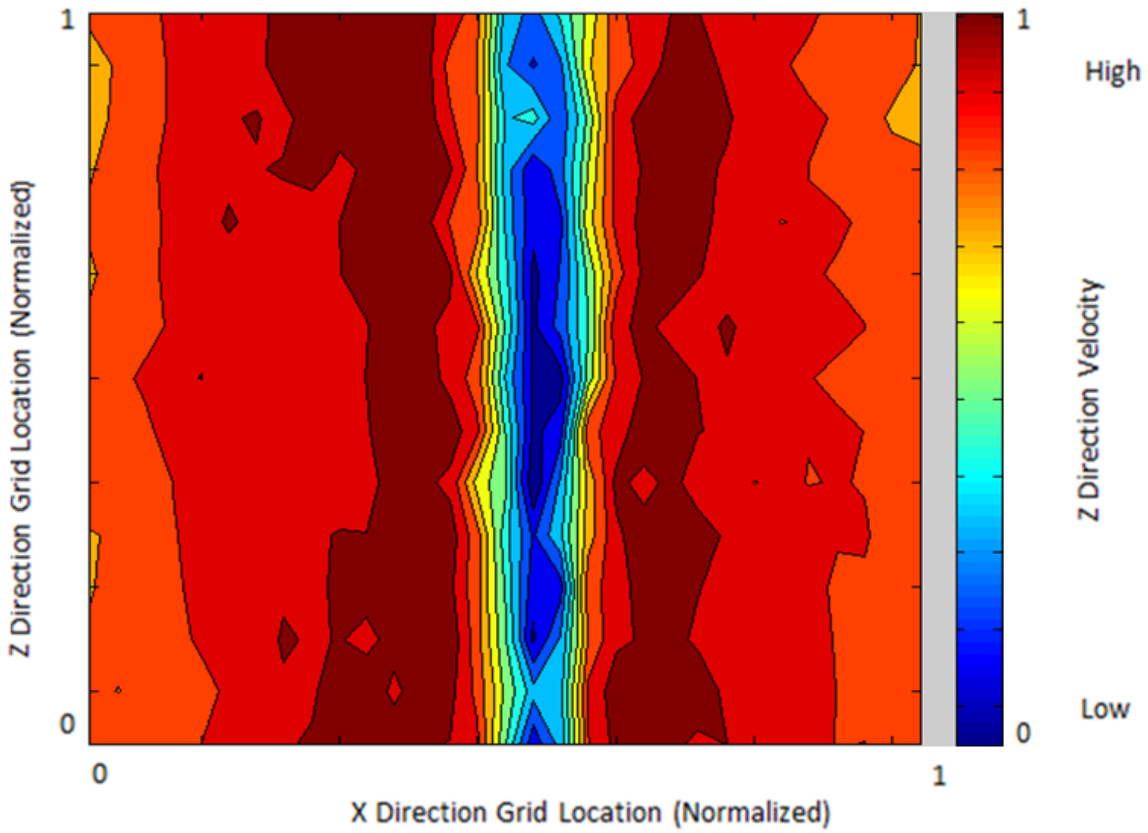

Figure 43. 78.74 cm by 38.1 cm horizontal grid 15.24 cm behind turbine and 7.62 cm above the wind tunnel floor

The horizontal grid shown in Figure 43 starts 15.24 cm behind the wind turbine and is 7.62 cm above the floor of the wind tunnel. At this level the wind turbine support dominates the flow and does not dissipate rapidly.

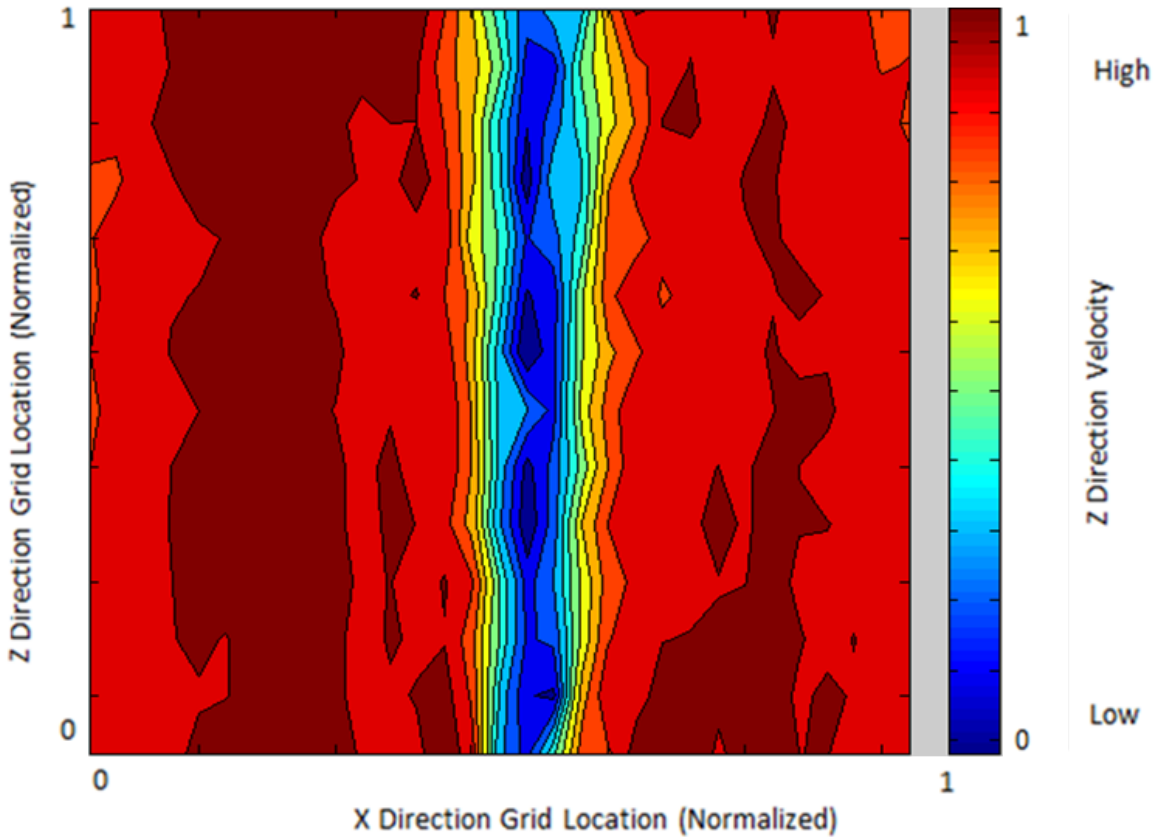

Figure 44. 78.74 cm by 38.1 cm horizontal grid 15.24 cm behind turbine and 15.24 cm above the wind tunnel floor

Figure 44 shows that a horizontal plane at 15.24 cm is still very similar to the flow at 7.62 cm.

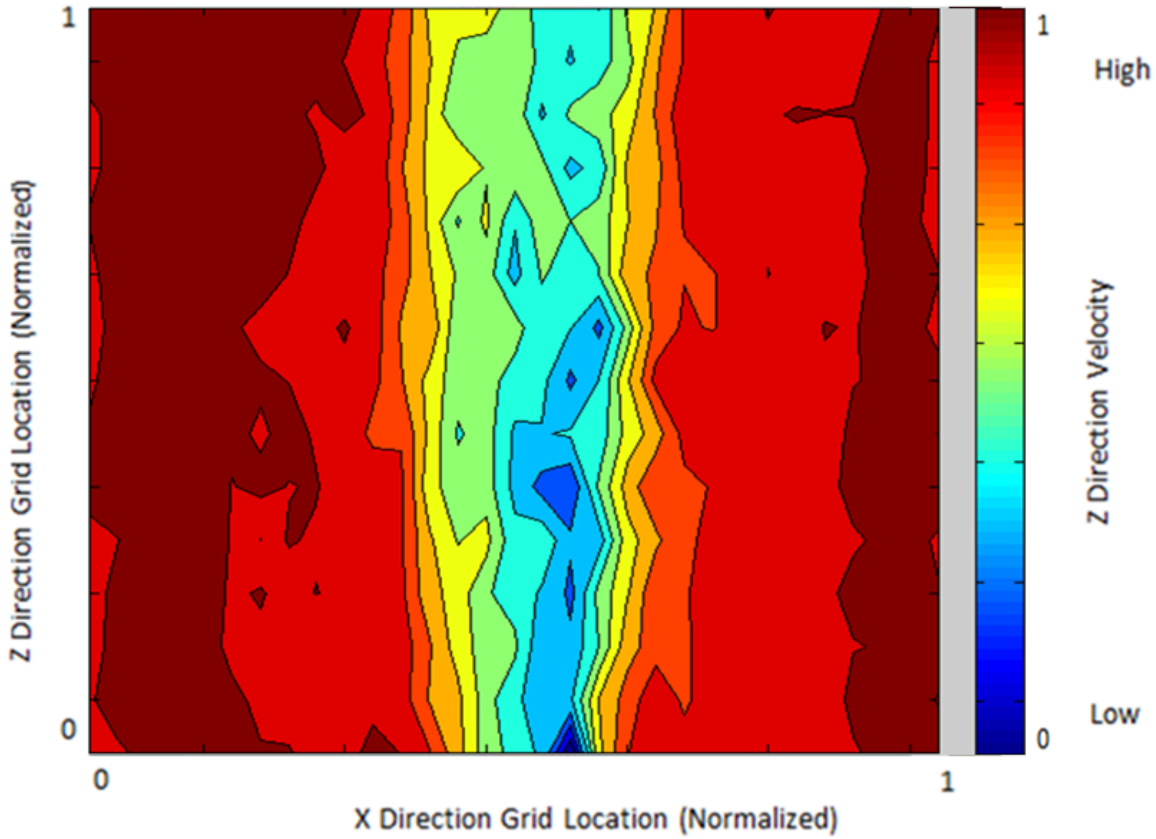

Figure 45. 78.74 cm by 38.1 cm horizontal grid 15.24 cm behind turbine and 30.48 cm above the wind tunnel floor

At 30.48 cm off the floor of the wind tunnel the velocity deficit caused by the support starts to be disrupted by the wind turbine blades. The structure is less uniform and more spread out as the two turbulent flows collapse into each other.

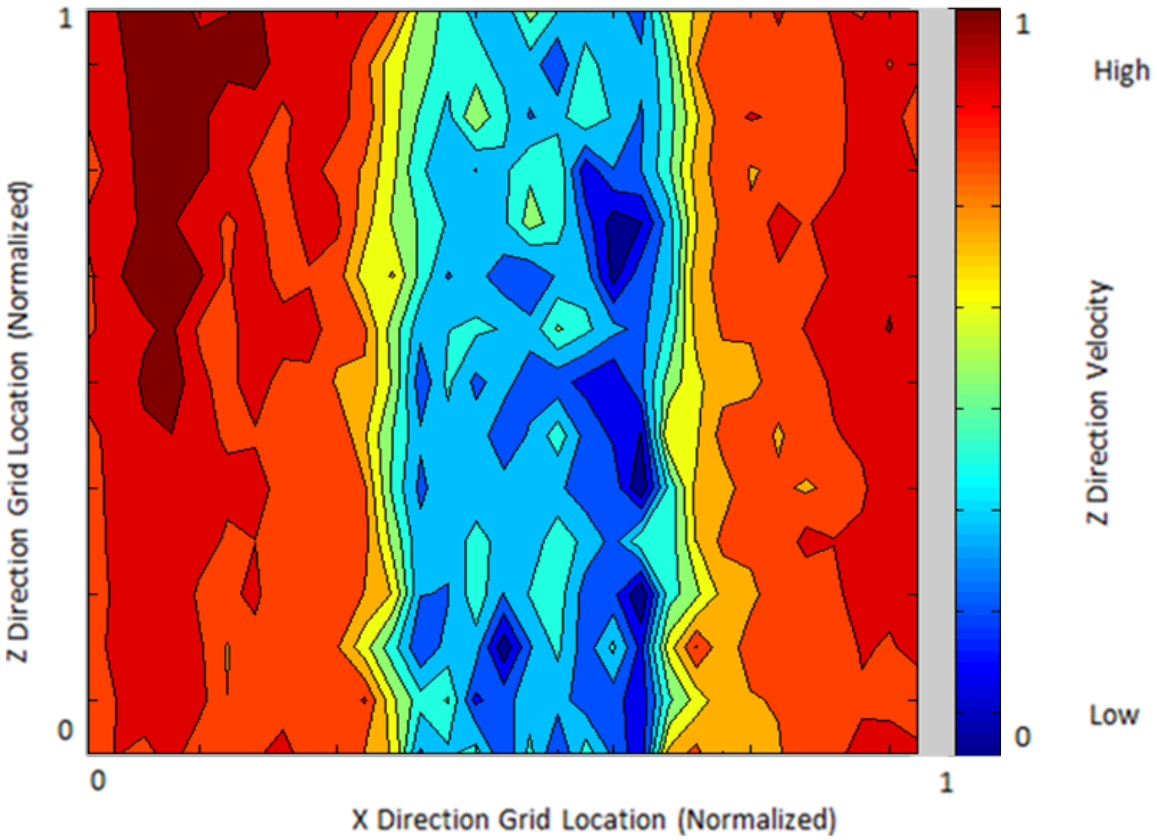

Figure 46. 78.74 cm by 38.1 cm horizontal grid 15.24 cm behind turbine and 45.72 cm above the wind tunnel floor

At 45.72 cm above the wind tunnel floor, the plane is behind the wind turbine blades. It is of note that even at 35.56 cm behind the wind turbine the velocity deficit region is getting smaller as it returns to ambient.

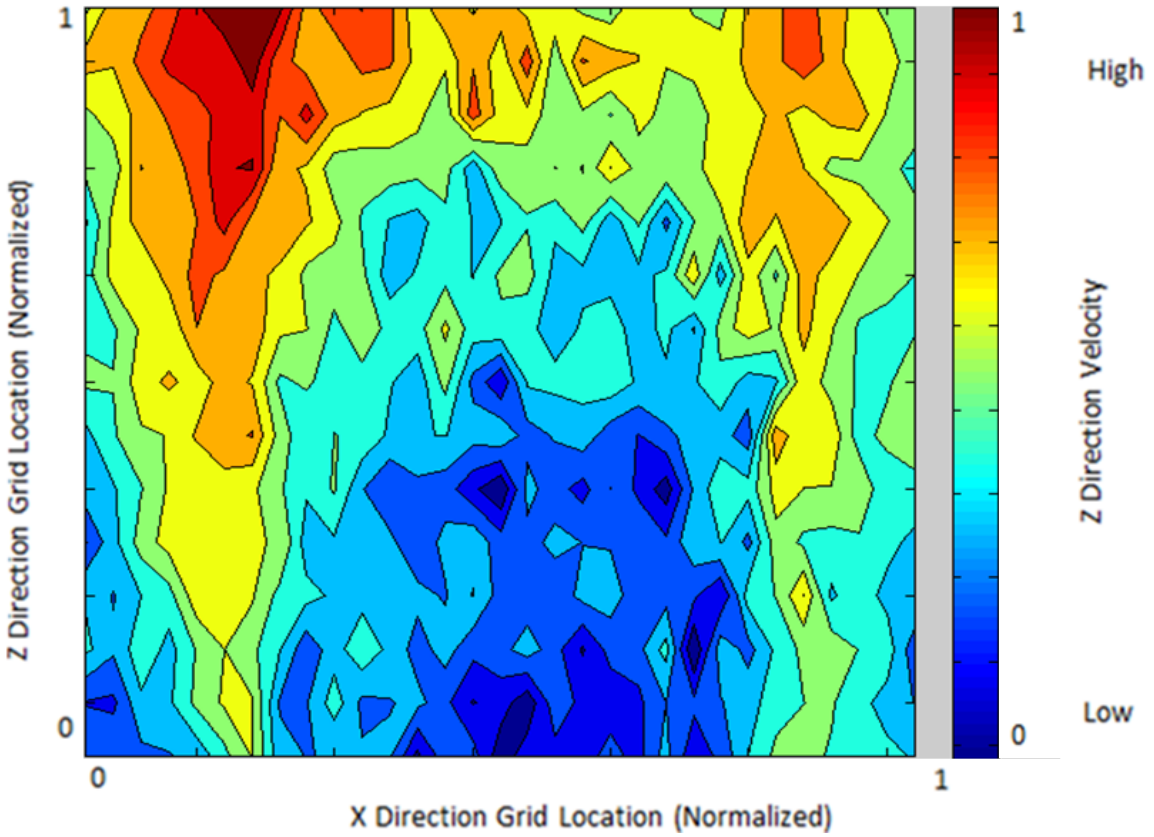

Figure 47. 78.74 cm by 38.1 cm horizontal grid 15.24 cm behind turbine and 60.96 cm above the wind tunnel floor

Figure 47 above is at 60.96 cm above the wind tunnel floor, approximately half way between the blade tip and the hub. Again, the velocity deficit begins to erode by 15.24 cm behind the wind turbine. However, the accelerated flow between 25.4 cm and 35.56 cm could be due to the wall effects creating flow channels with higher velocity air.

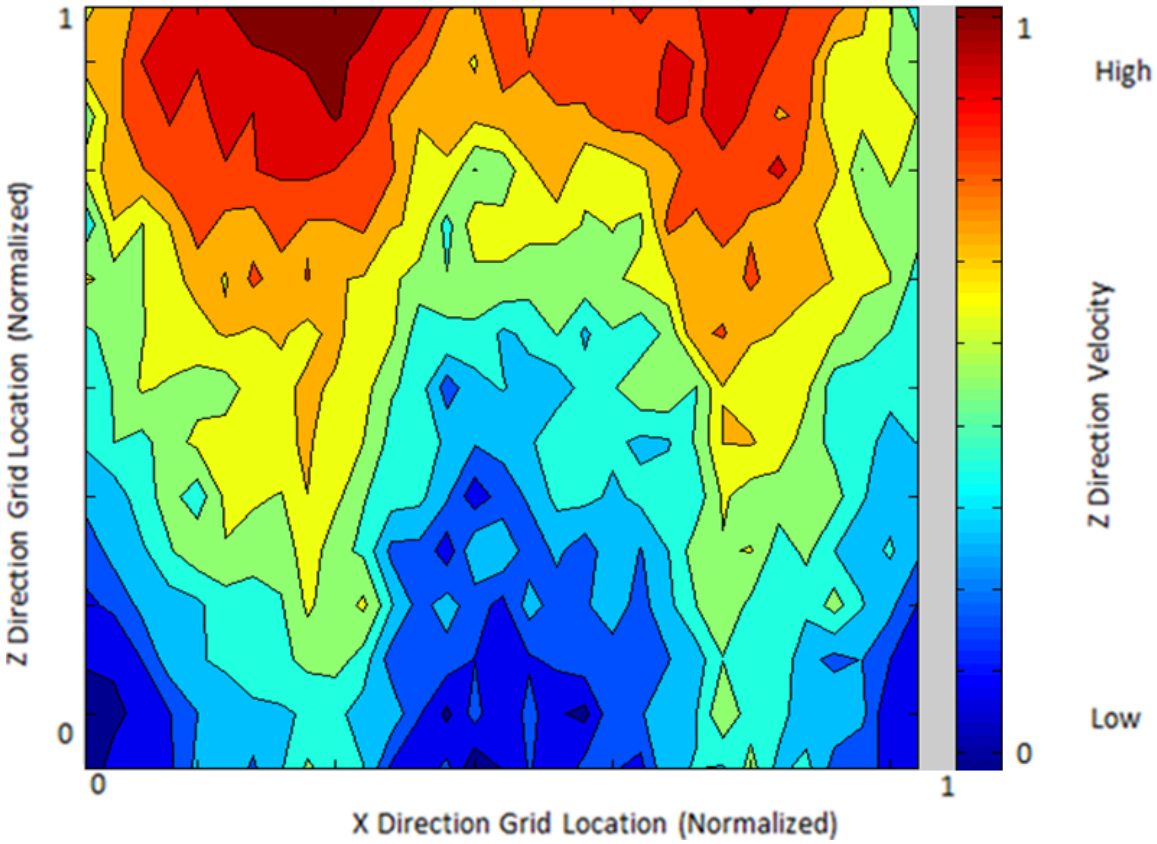

Figure 48. 78.74 cm by 38.1 cm horizontal grid 15.24 cm behind turbine and 68.58 cm above the wind tunnel floor

At 68.58 cm above the wind tunnel floor, at the blade tips, the flow structures observed at 60.96 cm are more exaggerated.

Conclusions:

Due to a deficit in available high wind land, increased pressure is being put on placing wind turbines closer and closer together. Additional emphasis is being applied to understanding the near and far wind turbine wake and the resulting unique structural loading that the wake causes on downwind wind turbines. To this end, this study focused on characterizing the wake structure through hotwire velocimetry and the design and construction of a low turbulence wind tunnel. A model wind turbine was also designed and constructed with NACA 4412 blades.

The results given throughout this study match with the theory very well. Measured planes in the near wake region had high velocity gradients behind the hub and at the blade tips. This matches the theory presented in **Error! Reference source not found.** as high velocity gradients are indicative of high turbulence intensity. High turbulence intensity can be seen due to the velocity deficit caused by the hub and slow moving portions of the blade. In addition, high velocity gradients are found at the blade tips due to the large velocity difference between the moving blades and the ambient flow. Similar results are witnessed in large scale wind turbine experimentation in Figure 3 and in LES simulation in Figure 6.

As the measurement planes move further away from the wind turbine plane, the minimum velocity in the flow increases as the flow returns to ambient. The flow structures also become more diffuse, less defined, and more spread out. This is indicative of the flow toward the edges returning to ambient and the turbulence collapsing in toward the center. This is shown in the far wake, 4 rotor diameters and higher, in the LES simulation results in Figure 6. In addition, the experimental results in Figure 4 show the velocity gradients degrading by 1 rotor diameter.

All horizontal planes measured show the flow moving toward returning to ambient within 15 to 30 cm, or 0.5 rotor diameters. This is accelerated from what is witnessed in field testing, however is similar to what researchers at ENSAM-Paris found in Figure 5. Wind tunnel wall effects accelerate the flow's return to ambient conditions. A test on a smaller wind turbine would somewhat negate these effects.

In the near wake it can be seen that down-wind wind turbines would experience widely varying turbulence structures. As predicted, in the far wake the turbulence collapses toward the center in a roughly bell shaped curve.

This study demonstrated the successful construction and operation of a new 1.2 meter test section wind tunnel to characterize the wake behind a 60 cm model wind turbine using hotwire velocimetry. These results can now be built upon to refine the wake characterization enabling the prediction of cyclical loading on downwind wind turbines.

Recommendations and Future Study:

Additional testing should be conducted on a smaller diameter wind turbine to explore the lengths of the transitions between the near and far wake and from the far wake to ambient. In addition, a downwind wind turbine with strain gauges on the blades should be tested to investigate the effects of different flow structures on the blades.

This experiment could be significantly improved with a fan designed for low turbulence wind tunnel applications. The current fan is the limiting factor on maximum wind tunnel flow velocity and is very noisy. Noise, if excessive enough, can cause turbulence in the wind tunnel and even flow separation in the contraction and diffuser sections.

The diffuser was designed to be temporary until a new fan was purchased. A more permanent diffuser should be installed in the future to allow for smoother flow into the fan.

In addition, time should be taken to optimize the number of screens used for flow conditioning in the wind tunnel. The current combination of six screens was the maximum recommended number of screens. It could be found through trial and error that fewer screens result in the same amount of turbulence reduction in the wind tunnel. This would reduce the pressure loss in the system and allow for higher maximum wind tunnel velocities.

Future recommended upgrades also include a three axis research grade hot wire anemometer and Particle Image Velocimetry (PIV).

Bibliography:

[1] Smith, Gillian, W. Schlez, A. Liddell, A. Neubert and A. Pena, "Advanced Wake Model for Very Closely Spaced Turbines," in *Proc. of European Wind Energy Conference*, Greece, Athens, 2006.

[2] T. Hahm and W. Steffen, "Turbulent Wakes in Wind Farm Configuration," T Ü V Nord, Systec Gmbh, Co Kg, Sciences, New York, 2006.

[3] Deutsches Institut fur Bautechnik DIBt, "Dynamic Loads in Wind Farms I; Final report Joule Project," *Untersuchung des Nachlaufes von Windenergieanlagen und dessen Auswirkung auf die Standsicherheit der benachbarten WEA in Parkaufstellung; Forschungsvorhaben,* pp. 32-5-3.78-1007/02, 1992.

[4] F. Massouh and I. Dobrev, "Exploration of the Vortex Wake behind of Wind Turbine Rotor," *Journal of Physics: Conference Series 75,* p. 012036, 2007.

[5] Hattori, Yasuo, M. Yamamoto, T. Eguchi, K. Kondo, H. Suto and N. Tanaka, "A Wind Tunnel Experiment on Wake Structure of a Wind Turbine," KAJIM Technical Research Institute, Kajim.

[6] Jimenez, Angel, A. Crespo, E. Migoya, J. Garcia and F. Manual, "Large Eddy Simulation of a Wind Turbine Wake," Technical University of Madrid, Madrid.

[7] Barlow, B. Jewel , W. H. Rae and A. Pope, Low-speed Wind Tunnel Testing, New York: Wiley, 1999.

[8] P. Bradshaw and R. D. Mehta, "Design Rules for Small Low Speed Wind Tunnels," *The Aeronautical Journal of the Royal Aeronautical Society,* pp. 443-49, 1979.

[9] R. I. Loehrke and H. M. Nagib, "Control of Free-Stream Turbulence by Means of Honeycombs: A Balance Between Suppression and Generation," *Journal of Fluids Engineering,* p. 342, 1976.

[10] J. Scheiman and J. D. Brooks, "Comparison of Experimental and Theoretical Turbulence Reduction from Screens, Honeycomb, and Honeycomb-Screen Combinations," *Journal of Aircraft,* pp. 638-43, 1981.

[11] H. L. Dryden and B. G. Schubauer , "The Use of Damping Screens for the Reduction of Wind-Tunnel Turbulence," *Journal of the Aeronautical Sciences,* pp. 221-28, 1947.

[12] R. D. Mehta, "Turbulent Boundary Layer Perturbed by a Screen," *AIAA Journal,* Vols. 23, No.

9, September 1985.

[13] P. Bradshaw and R. Pankhurst, "The Design of Low-speed Wind Tunnels," *Progress in Aerospace Sciences 5,* pp. 1-69, 1964.

[14] J. E. Finn, "How to Measure Turbulence (Practical Guide)," 2002. [Online]. Available: http://www.dantecdynamics.com. [Accessed June 2012].

[15] M. O. L. Hansen, Aerodynamics of Wind Turbines, London: Earthscan, 2008.

[16] K. G. Rados, J. M. Prospathopoulos, N. C. Stefanatos, E. S. Politis, P. K. Chaviaropoulos and A. Zervos, "CFD Modeling Issues of Wind Turbine Wakes Under Stable Atmospheric Condition," in *Proc. of European Wind Energy Conference*.

[17] Ott, Soren, A. Sogachev, J. Mann, H. E. Jorgensen and S. T. Frandsen, "Applying Flow Models of Different Complexity for Estimation of Turine Wakes," Wind Energy Department, Riso-DTU.

[18] S. Aubrun, P. Devinant and G. Espana, "Physical Modelling of the Far Wake From Wind Turbines," Laboratoire De Mecanique Et D'Energetique.

[19] J. N. Sorensen, R. Mikkelsen and N. Troldborg, "Simulation and Modelling of Turbulence in Wind Farms," Department of Mechanical Engineering-Technical University of Denmark, Denmark.

[20] Pascheke, Frauke and P. E. Hancock, "Wake Development and Interaction Within an Arrray of Large Wind Turbines," University of Surrey, Guildford.

[21] A. Pope and W. H. Rae, Low-speed Wind Tunnel Testing, New York: Wiley, 1984.